

1988 Annual Report

NAGW-872

Consortium for Materials Development in Space

N89-22773

Unclas
0201510

G3/29

(NASA-CR-181405) CONSORTIUM FOR MATERIALS
DEVELOPMENT IN SPACE Annual Report, 1 Oct.
1987 - 30 Sep. 1988 (Alabama Univ.) 48 p

CSCI 22A



Industrial members of CMDS are:

**Boeing Aerospace Company
Deere & Company
McDonnell Douglas Astronautics Co., Huntsville
Teledyne Brown Engineering
Wyle Laboratories
IBM (Almaden Research Center)
Frontier Research**

On the front cover: UAH graduate student Brian Benson maneuvers in free-fall aboard NASA's KC-135 low-g aircraft as he operates a forerunner of the apparatus designed for the electrodeposition experiment planned for flight on Getaway Special GAS 105 in 1990 (see page 13).



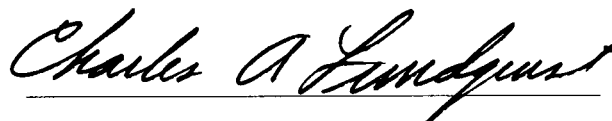
Consortium for Materials Development in Space

The University of Alabama in Huntsville
Huntsville, Alabama 35899

**Annual Report
Technical Section
Oct. 1, 1987-Sept. 30, 1988
NAGW-812**

Submitted by the University of Alabama in Huntsville ,
the legal entity responsible for establishing and operating the Consortium, to:

Market Development Branch,
Commercial Development Division,
Office of Commercial Programs,
National Aeronautics and Space Administration
Washington, DC 20546

A handwritten signature in black ink, reading "Charles A. Lundquist". The signature is written in a cursive style with a horizontal line underneath it.

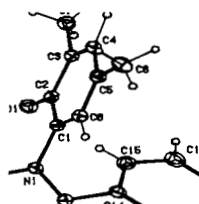
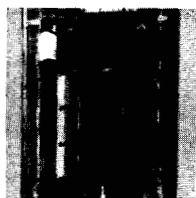
Charles A. Lundquist
Director, CMDS

Francis C. Wessling
Associate Director

James K. Baird
Principal Science Advisor

ORIGINAL PAGE IS
OF POOR QUALITY

CONTENTS



1

Fiscal Year Overview

The Consortium for Materials Development in Space (CMDs) has operated since 1985. This report reviews the Consortium status after that time, with emphasis on accomplishments during the third year.

From its beginning, the Consortium embraced a project structure and continues to operate primarily in that mode. Table 1-1 gives some features of the adopted project concept as it has been presented on many occasions. The Consortium status and technical accomplishments are largely those of the individual projects. Accordingly, later parts of this document contain individual project reports.

Table 1-1

CMDs project characteristics

- The principal activities of the Consortium are organized into several individual projects that are reviewed and accepted by the Consortium Council.
- Each project typically involves a member industry and a specialized co-investigation team from a member university.
- The implementation plan and contractual agreements for each project are treated individually between the participants so that proprietary rights are protected.
- The ultimate commercial utilization of the products of a project normally is the privilege and responsibility of the industrial participant(s) in that project.

Table 1-2 lists the projects and some rudimentary facts about each as of Sept. 30, 1988. As the individual reports show, the projects have made respectable progress. One strong manifestation of this is the inventory of equipment for operation in space. However, other progress has been limited by the hiatus of space flight opportunities. The successful resumption of Space Shuttle missions on Sept. 29, 1988, was an auspicious end to this reporting period and a welcome encouragement that future reports will discuss results from shuttleborne equipment.

Shuttle flights are not the only

option for access to space. Although limited in reduced acceleration periods, suborbital sounding rockets offer a relatively quick and inexpensive path to space experimentation. For that reason, early in this fiscal year, the Consortium began development of a rocket payload. Table 1.3 and Figure 1-1 show the elements of this payload, and subsequent project reports give further details for the individual experiments. A further section of this document describes the integration of the payload.

In mid-summer, the NASA Office of Commercial Programs informed the Consortium that it would support procurement of a suborbital rocket and launch services from a commercial source in the United States. This move has two benefits for commercial development—it provides an early flight opportunity for the materials projects in Table 1-3, and it advances the evolution of the commercial rocket launch industry in the United States. It also re-establishes for the nation a suborbital rocket option for subsequent materials experiments. Such a continuing capability has been employed productively by other nations in recent years.

To pursue these goals, the Consortium established and followed the schedule in Table 1-4. Space Services Incorporated (SSI) of Houston, Texas, was selected as the rocket contractor during the last days of the fiscal year. Launch was targeted for March 1989 from White Sands Missile Range, N.M. Contractual negotiations and technical planning meetings with SSI began during the first week of October.

Hence, during the 1988 Consortium fiscal year, preparation for the suborbital rocket mission (to be called Consort 1) was a predominant activity. As described above, this included:

1. Individual experiment definition, design and fabrication,
2. Total payload definition, design

and integration, and

3. Rocket and launch services specification, solicitation and contractor selection.

As the end of the fiscal year approached, payload planning information for future Space Shuttle flights became available. For example, the Marshall Space Flight Center requested specifications and requirements for equipment planned for U. S. Materials Lab 1 (USML-1). In reply, on Sept. 13, 1988, the Consortium provided the requested information for an integrated rack of equipment to support

several of its projects. This effort is discussed presently.

Also, the resumption of Shuttle flights motivated renewed attention to Getaway Special (GAS) #105. Activity on this multiple experiment package had been intense in the two previous fiscal years, but had slacked off in this fiscal year. The reduced activity recognized in part that many tasks had been completed and in part that Consort 1 could provide an earlier flight opportunity for some experiments. The status of GAS 105 also is summarized in this report.

Table 1-2

CMDS Materials Projects				
Project or task	Remarks	Industry Partner	Potential Products	Early Carriers
Surface coatings and catalyst production by electrodeposition	Original project	McDonnell Douglas Astronautics	Improved surface coatings and metal catalysts	Consort 1, GAS 105, USML-1
Physical vapor deposition growth	Original project	Boeing Aerospace	ZnSe electro-optical devices	Shuttle middeck furnace
Non-linear optical organic materials	Original projects	IBM & Teledyne Brown Engineering	Optical computers and electrooptical devices	GAS 105, USML-1
Chemical processing of organic materials	Original project	Phillips Petroleum (Chief Investigator)	Blended polymers and separation of organic materials	Consort 1, GAS 105, USML-1
Nuclear track detectors	New project (1987)	Frontier Research	Improved detector materials	GAS 105
Spacecraft surface coatings	Original project	Boeing Aerospace (Chief Investigator)	Spacecraft surface coatings	LDEF, ECOM-3
Powdered metal sintering	Original task; now a project	TBE and Teledyne Wah Chang	Composites of metals and refractory materials	Consort 1
Spacecraft systems for commercial satellites	Original task	Boeing Aerospace	Spacecraft systems for commercial satellites	Everest geostationary satellite test
Wake shield	Original task; Status TBD	Wyle Laboratories	Purified metals	TBD
Lightweight space structures	Original task	Boeing Aerospace	Lightweight space structures	Consort 1
Iron-carbon Solidification	Original task	Deere and Co.	Improved cast iron processes	future Consort

ORIGINAL PAGE IS OF POOR QUALITY

Table 1-3

Major elements of the Consort 1 payload

Experiment Equipment

Electrodeposition
Elastomer-modified epoxy resins
Demixing of immiscible polymers
Powdered metal sintering
Polymer foam formation
Materials Dispersion Apparatus

Support Equipment

MEA accelerometers
UAH accelerometers
Controller

Still further flight opportunities are subjects of serious consideration. These include later Consort flights, additional GAS carriers, Spacehab, subsequent Materials Laboratories, other Shuttle accommodations, the Commercially Developed Space Facility, and eventually Space Station. It is premature to present detailed plans for these now, but their importance to the long range goals of the Consortium is great.

An urgent task for next fiscal year is a revised development plan and timeline for each project showing what space carriers will be employed and how improved equipment can evolve from flight to flight. Such plans are timely now that flight manifest information is becoming available. The attention given recently to manifest questions by the Office of Commercial Programs will greatly facilitate this necessary planning. The column titled "Early Carriers" in Table 1-2 gives initial

thoughts on this topic.

Finally, a fiscal year overview must include pertinent organizational and administrative matters. The organization chart for the Consortium has changed little (Figure 1-2). One change is the added function of Consort 1 Project Manager, undertaken as a dual role by the Associate Director. Another addition is the USML-1 Interface Engineer.

The Consortium Council met twice, on Dec. 8, 1987, and on April 26, 1988. At the first of these meetings, the Council redefined the classes of Consortium membership. There are now three:

- Member of the Council
- Member-at-Large (non-voting in Council)
- Associate Member (project or task participant only)

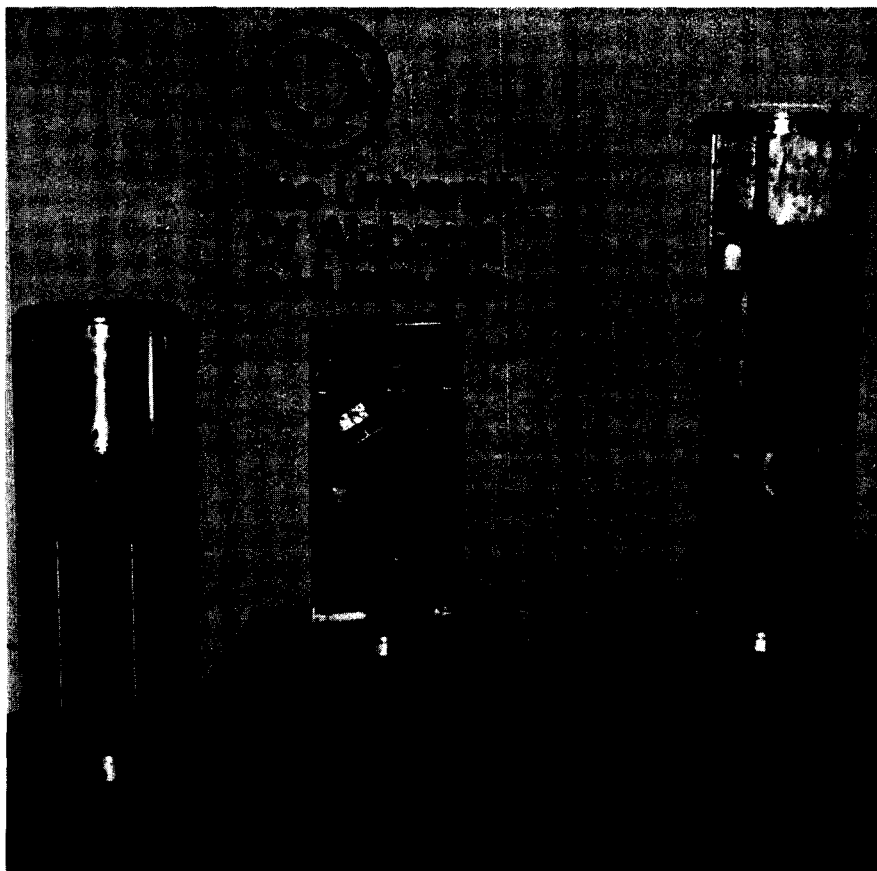
The detailed requirements for these classes of membership were further refined at the April Council meeting. Also at its December meeting, the Council accepted two new Associate Members: Frontier Research and IBM (Almaden Research Center).

The composition of the Consort 1 payload led to new CMDS participants in consulting and guest investigator roles. These are Phillips Petroleum Company (Industrial Guest Investigator); Hercules Incorporated (Industrial Consultant); Instrumentation Technology Associates (Industrial Guest Investigator); University of California (Paul Concus, Lawrence Berkeley Laboratory, Guest Investigator).

The third CMDS Scientific and Technical Workshop was held April 26-28, 1988, at Lake Gunter State Park Lodge. This is the annual workshop at which each project

Figure 1-1

Consort 1 payload on display for the preproposal briefing.



presents its progress and plans (excepting proprietary details). Time is allotted for questions and discussions. This workshop is one primary mechanism for cross-communication between projects.

During the year, the Consortium Director and Associate Director represent the Consortium at many pertinent meetings. A high point of these was the NASA Office of Commercial

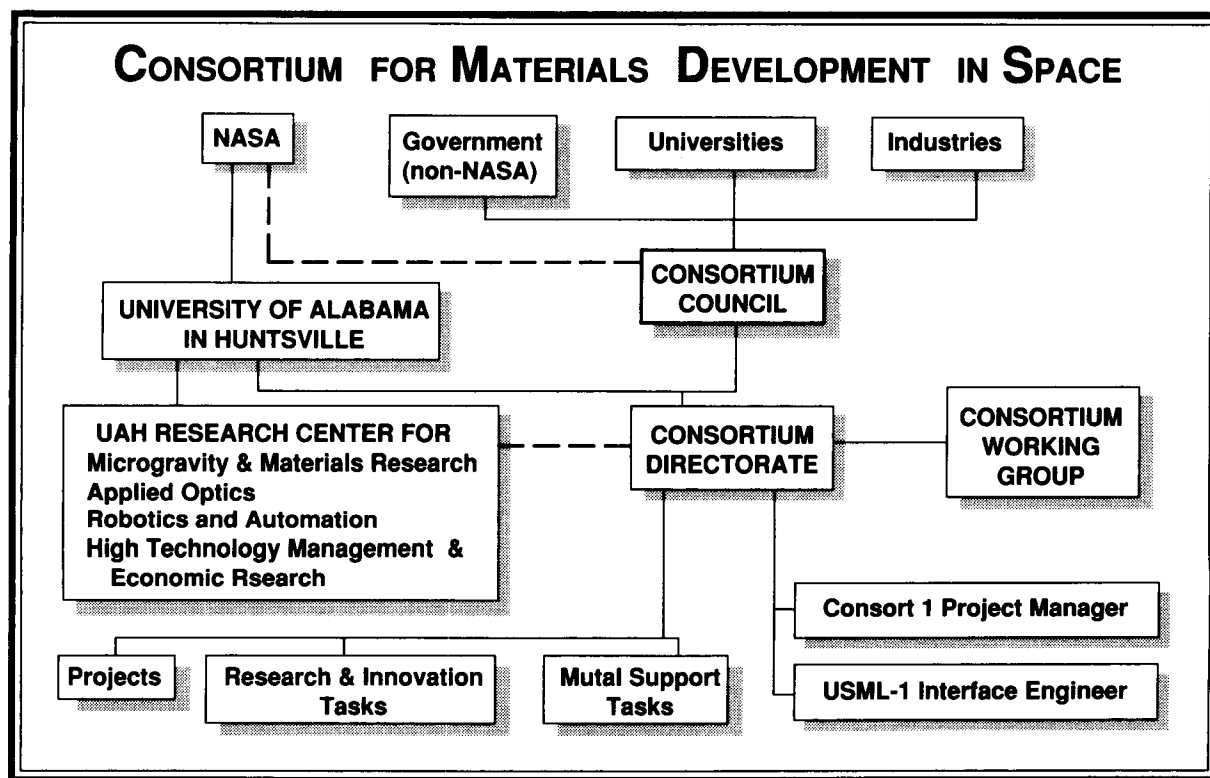
Programs, Centers for Commercial Development of Space, Operations Management Workshop (Williamsburg, Va., August 1988). During this workshop, a coordinated, inter-CCDS approach to common topics was solidified. This mechanism promises to strengthen individual CCDS programs through a facile exchange of ideas and appropriate cooperative actions.

Consort 1 Procurement Schedule

Solicitation to industry	July 29
Preproposal briefing	Aug. 16
Proposals received	Sept. 16
Proposals evaluated	Sept. 28

Table 1-4

Figure 1-2



2 Consort 1

ORIGINAL PAGE IS
OF POOR QUALITY

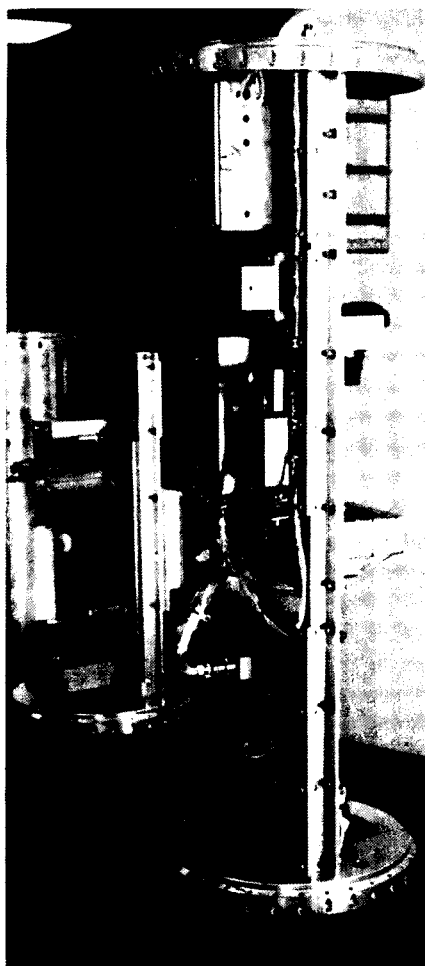


Fig. 2-1
*Central section of the Consort 1
payload showing mounting struc-
ture.*

To perform extended low-g experiments at the earliest opportunity, CMDS in 1988 elected to develop a suborbital sounding rocket flight, now called Consort 1. This flight will carry experiments supporting specific Consortium projects and one industrial apparatus incorporating dispersion investigations for several clients.

NASA's Office of Commercial Programs in January 1988 authorized the Consortium to proceed with the development of this rocket payload for materials investigations, after considering a plan submitted by the Consortium. The six selected experiment packages, plus two accelerometer systems and a controller, are integrated into a payload 17.26 inches in diameter and 11.5 feet long, and weighing about 650 pounds. The payload elements are contained in three cylindrical sections which are mounted end-to-end (Figure 2-1).

The experiment units and investigators are:

1. Demixing of immiscible polymers, J. Milton Harris of UAH and Paul Concus of the University of California at Berkeley (page 23),
2. Elastomer-modified epoxy resins, J. Milton Harris and Francis Wessling of UAH and Jon Geibel of Phillips Petroleum Co. (page 40),
3. Foam formation in low gravity, Samuel McManus and Francis Wessling of UAH and Deborah Weiker of Hercules Inc. (page xx),
4. Electrodeposition, Clyde Riley of UAH and George Maybee of McDonnell Douglas Astronautics (page 39),
5. Powdered metal sintering, James Smith of UAH and Tripty Mookerji of Teledyne Brown Engineering (page 31), and
6. Materials Dispersion Apparatus, John Cassanto of Instrumentation Technology Associates of Malvern, Pa.

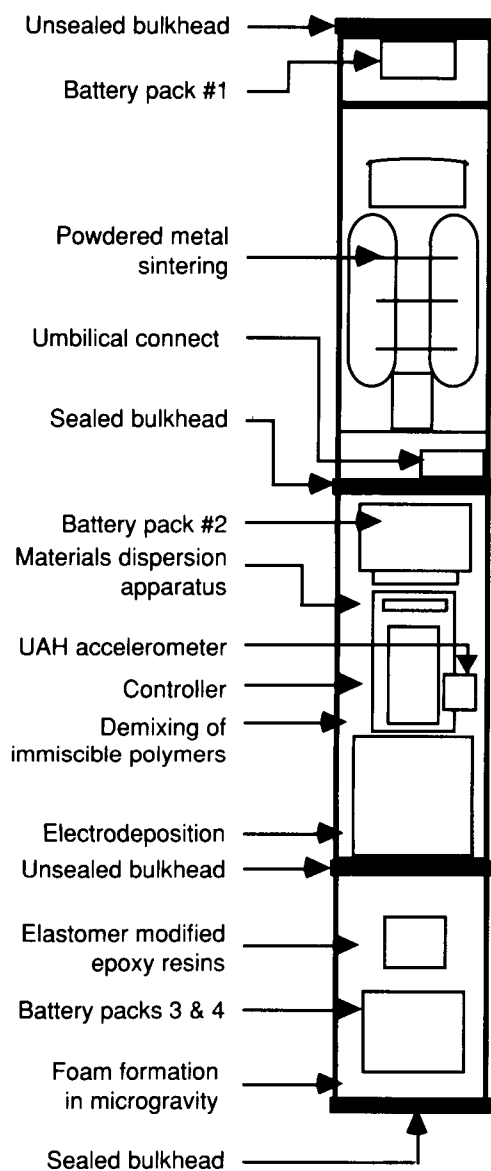
Detailed descriptions of the CMDS investigations are on the indicated pages. The Materials Dispersion Apparatus (MDA) is designed to allow mixing or dispersion of samples in 180 pairs of cells recessed in the adjoining faces of two sliding blocks. Before launch the cavities are offset so the samples are kept separate. At the start of free fall, a drive motor shifts the two blocks so the cavities are aligned and the samples may disperse between adjacent halves. Before the onset of re-entry forces the blocks are again moved out of alignment to isolate samples for post-flight analysis. Table 2-1 lists the investigations to be conducted in the MDA and the responsible parties.

In addition, two accelerometer packages will be carried to measure low-g accelerations along three orthogonal axes. The first accelerometer package, developed jointly by Jan Bijvoet of CMDS and Robert Newberry, a UAH student, will provide high bandwidth analog data. It is backed up a second set of accelerometers, loaned by Marshall Space Flight Center, which flew on the Materials Experiment Assembly, to provide narrow-bandwidth digital data. Bijvoet is the investigator for the MEA accelerometer project. The two packages will provide a quantitative measure of the micro-acceleration levels experienced by the experiment packages during unpowered flight. Data from both packages will be telemetered to the ground and processed to determine the micro-gravity level and vector at the experiment location. It is anticipated that accelerations will be less than 10^{-5} g during the coast phase.

The controller is derived from a design developed initially for GAS 007 by the Marshall Amateur Radio Club. Charles C. Rupp of that Club has provided valuable continuing support for the rocket version of the controller. While not as powerful as many desktop computers, it is more than adequate for the tasks required

Figure 2-2
Consort 1 payload and launch vehicle

**University of Alabama in Huntsville
 Consortium for Materials Development in Space
 Consort 1/Starfire 1**



**CONSORT 1
 Payload
 (CMDS)**

**Guidance, Telemetry
 & Recovery Systems**

**Sustainer
 Stage**

**Booster
 Stage**

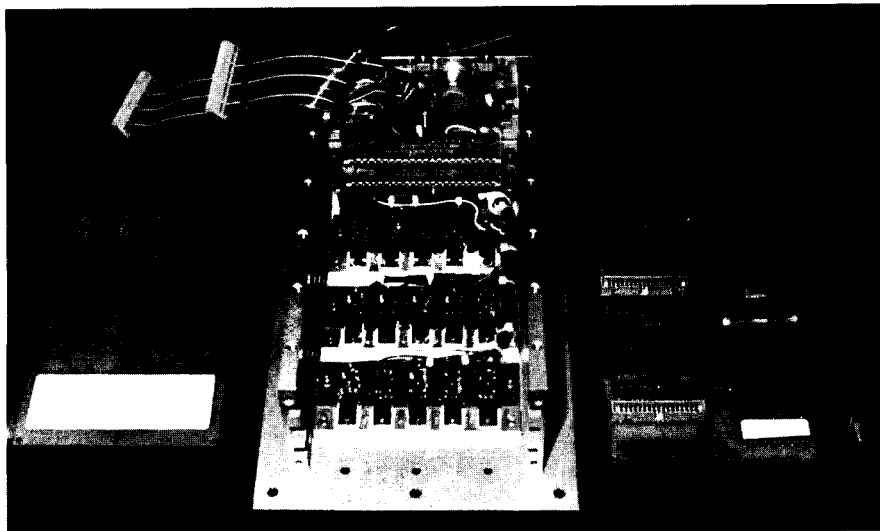
**STARFIRE 1
 Launch Vehicle
 (SSI)**

**(Payload integrated by
 McDonnell Douglas Space Systems Co.)**

(Drawing by McDonnell Douglas and Space Services Inc.)

Figure 2-3

Consort 1 controller with single-board computer (right) and accelerometer interface (left).



on Consort 1. It uses a low-power, high-performance, single-board computer for control processing and data logging. The CPU is a National Semiconductor Corp. NSC800 (Z-80 compatible) running at 2 MHz. The program is stored in a 32K EPROM and data are stored in 32K of RAM. It handles 32 channels of analog input

plus a single serial port and two parallel ports.

During 1988 the payload for this flight was assembled at UAH with the assistance of McDonnell Douglas Astronautics Co. in Huntsville. Vibration tests were then conducted at Wyle Laboratories, also in Huntsville. Significant support for the Consort project has been provided by NASA's Lewis Research Center, Wallops Flight Facility, and Marshall Space Flight Center.

The Starfire 1 vehicle to be provided by Space Services Inc. is a two-stage vehicle using a Thiokol booster (derived from the U.S. Navy's SM-2 missile) and a Black Brant VC sustainer motor. It stands 52.3 feet tall and weighs about 6,000 pounds at liftoff.

The Consort 1 mission will be similar to suborbital materials science flights carried out by the United States and other nations since the mid-1970's. After sustainer burnout the rocket is despun and stabilized. Low-g conditions (10^{-5} g or less) start at T+73 seconds and an altitude of 68 miles. The rocket's apogee will be about 200 miles. This provides about 7 minutes of low-g conditions as the payload coasts into space then back to the atmosphere. All experiments are terminated when the rocket falls back to 68 miles and g-forces start rising. The payload parachutes to Earth and is recovered for analysis of the processed samples and refurbishment of the experiment hardware.

Launch is planned in March 1989 at the White Sands Missile Range in New Mexico from a Navy/NASA launch pad. Additional flights may be sought depending on the results from Consort 1.

The project manager for Consort 1 is Francis Wessling.

Table 2-1

MDA experiments aboard Consort 1

#	Experiment	# Wells	Investigator
1	Solid/liquid diffusion in weightlessness	2	TBE/Mike Fisk
2	Bone marrow studies; (synovial fluid studies)	2	Rantek/William Vardamann
3a	Collagen polymerization	2	Bioserve*/Louis Stodieck
3b	Tubulin assembly	2	Bioserve*/Louis Stodieck
3c	Fibrin clot formation	2	Bioserve*/Louis Stodieck
4	Cell fixation	21	PSU*/Rich Hammerstedt
5	Inorganic crystal size in 0-g	1	PSU*/Martin Shoonen
6	Protein crystal stability	7	ITA/Rich Korzun
7a	Turbulent mixing	7	NBS/Paul Todd†
7b	Electrophoretic transfer	12	NBS/Paul Todd†
7c	Capillary flow	7	NBS/Paul Todd†
7d	Phase rearrangement	7	NBS/Paul Todd†
7e	Phenytoin precipitation	21	NBS/Paul Todd†
7f	Ceramic membrane formation	18	NBS/Paul Todd†
7g	Nafion membrane formation	21	NBS/Paul Todd†
7h	Chitosan formation	14	NBS/Paul Todd†

* Center for Commercial Development of Space
† Experiment administrator
NBS: National Bureau of Standards
PSU: Pennsylvania State University

ORIGINAL PAGE IS
OF POOR QUALITY

PERMANENT RECORD OF HIGH QUALITY

As now configured, Getaway Special 105 (GAS 105) contains equipment to support five CMDS projects. Initial planning for GAS 105, predating establishment of the Consortium, embraced a joint effort between UAH and the Space & Rocket Center as a sequel to GAS 007 flown successfully on the STS 61-C mission in 1985 (Figures 3-1, 2). GAS 007 carried out several student experiments and a communications experiment for the Marshall Space Flight Center Amateur Radio Club. As part of this heritage, a single student experiment is also included in GAS 105. Also, several electrical and mechanical support systems are derived from systems provided on GAS 007.

The NASA Getaway Special has been a popular payload programs because of its low cost and simple interface. The "GAS can" has a diameter of 20 inches and height of 28.5 inches; a volume of 5 cubic feet; and can contain up to 200 pounds of payload. The canister is mounted in the Space Shuttle payload bay and operates by a simple on/off command during the mission.

Four of the Consortium experiments on GAS 105 utilize the microgravity environment of space, and one requires exposure to the radiation environment. Consortium investigations are:

1. Separation of aqueous phases, (page 23),
2. Organic thin films, (page 22),
3. Organic crystals, (page 21),
4. Electrodeposition and codeposition, (page 13), and
5. Nuclear track detector materials, (page 38).

The scientific investigations involved in each of these is described on the indicated pages. A single student experiment, a follow-on from GAS 007, a yeast experiment, will also be carried.

In addition, the Marshall Amateur Radio Club participated in preparing an electronics package to provide power, control, and data systems.

This system has evolved directly from the system developed by for GAS 007.

To satisfy minimum experiment requirements, GAS 105 needs 48 hours of operation in the low-g environment of space; 96 hours is optimal. Experiments 1 and 4 can obtain significant results in as little as 10 hours, while Nos. 2 and 3 will yield their best results in 96 hours. The cosmic ray experiment will benefit proportionally to time in orbit.

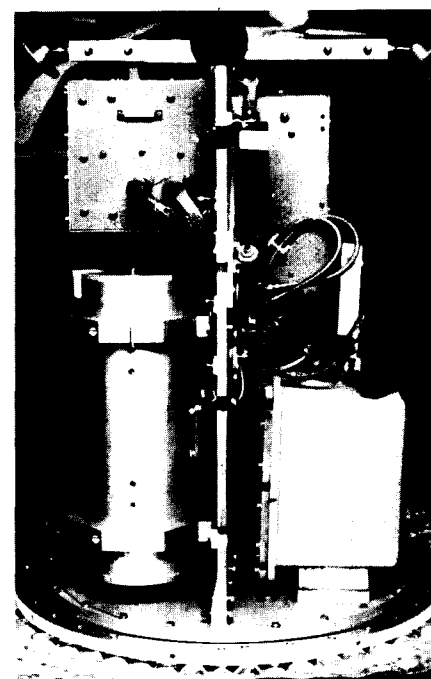
Each experiment has a timed sequence of operations that is programmed in the controller. These are described by investigation:

1. Separation of aqueous phases is conducted in 12 glass cells in a 2.4x5.6x6.9 cm package. Mechanical stirrers are turned on for 20 seconds to mix the liquid samples thoroughly, then turned off. Over the next 10 hours the separations of the immiscible fluids are photographed periodically by a 35mm camera using a strobe light mounted behind the cells. A resistive strip heater will maintain temperatures near 5°C before and after the experiment, and near 25°C during the experiment. An over-temperature cut-off relay protects the apparatus from a runaway heater.
2. Organic thin films are grown in two 1x4-inch evacuated quartz reaction cylinders mounted in an oven 3.5 inches in diameter and 14 inches long. The monomeric organic source material is coated on a glass-and-ceramic honeycomb, with a resistance heater to hold its temperature at 80°C (Figure 3-3). A cooled flat plate is at the other end. When the two are at their target temperatures, vapor of an organic material will pass from the hot end to the cold end and be deposited on the flat plate. It is estimated that transport of all the source material will take 96 hours, at which time the temperature will be reduced.

3

Getaway Special 105

Figure 3-1
GAS 007 before installation in GAS canister for flight.



ORIGINAL PAGE IS OF POOR QUALITY

Figure 3-2

Typical installation of Getaway Specials on Shuttle mission 61-C.



3. Organic crystals are grown in two ovens identical to those of experiment No. 2. The cylinders will be heated to 137 and 140°C at opposite ends in one tube, and to 147 and 150°C in the other. The seed material, coated on a glass-and-ceramic honeycomb at one end, will be vaporized, travel the length of the tube, and crystallize on a seed crystal at the other end. The objective is to grow a single crystal. This also requires 96 hours of processing for maximum benefit.
4. Electrodeposition and codeposition take place in eight electrodeposition cells mounted in a bank of transparent cells; two cells have electric stirring motors to agitate inert particles placed in solution. Like Experiment No. 1, the stirrers will be turned on to mix the fluids for 20 seconds. After stirring, the electrodes in the cells will be powered for five hours. The codeposition process will be photographed during this period and for an hour after the electrodes are turned off. Temperatures will be maintained near 5°C before and after the experiment, and near 20°C during the experiment. Electrical current for each cell, voltage for one cell, and temperature of the whole array will be displayed on a bank of LED's mounted adjacent to the cells. Ray Cronise, a UAH graduate student, is supported as a co-investigator in this work by a grant from Westinghouse.
5. Nuclear track determination uses a 15-cm cube of stacked emulsion plates of silver bromide gel, Lucite, CR-39, X-ray film, lead, and nuclear emulsion film to test the effectiveness of new cosmic ray

detector materials. The plates are 1 to 2 mm thick and sealed inside Lucite and aluminum boxes. This package is completely passive and only requires that it be present in space. However, because the emulsion materials are sensitive to high temperatures (>30°C), a small, self-contained data logger will record emulsion temperatures before, during, and after flight. The sensitivity of the new detector materials will be compared with that of standard materials.

The controller will operate the GAS 105 experiments after activation by the flight crew. It uses a CMOS microprocessor with a 32K-byte data memory, 32K-byte EPROM main program memory, and 128 bytes temporary memory (scratch pad). Two AA alkaline cells provide backup power to the CMOS memory whenever the main power is off. Primary power is supplied by a 45-pound Shuttle Solid Rocket Booster battery.

The experiments are mounted on both sides of a divider plate that extends from top to bottom of the GAS can. The electrodeposition and cosmic ray packages occupy one side; the two crystallization experiments, battery, and the controller occupy the other side.

During this year the design of GAS 105 was completed (the final safety data package submitted to NASA in for review and approval). Components of GAS 105 are now in final assembly and test.

Flight readiness of GAS 105 is scheduled for Dec. 1, 1989. This anticipates that a flight opportunity is likely in the summer of 1990.

The integration manager is Francis Wessling of CMDS.

4

USML-1 Equipment

To make the widest possible use of facilities scheduled to fly aboard the U.S. Microgravity Laboratory (USML) missions, NASA's Office of Commercial Programs in 1988 announced that some USML-1 resources would be available to the Centers for Commercial Development of Space.

The USML missions, scheduled to start in 1992, will use Spacelab, a pressurized, shirt-sleeve laboratory module which rides in the Space Shuttle payload bay. Experiments may be conducted in an environment comparable to a terrestrial laboratory. Experiment activities aboard the Spacelab 3 and D-1 missions in 1985 were similar to those planned for USML-1. Investigations planned by the CDMS are:

1. Non-linear optical organic crystals, (page 21),
2. Non-linear optical monomer thin films, (page 22),
3. Electrodeposition, (page 13),
4. Organic separation experiment, (page 23),
5. Elastomer modified epoxy resins, (page 40), and
6. Foam formation experiment, (page 39).

The scientific investigations involved in each of these is described on the indicated pages. Much of the hardware proposed will use designs developed for the Consort 1 and GAS 105 missions described on previous pages and should be mounted in a 40-inch, double-wide rack in the Spacelab module. Although several of the experiments will be automated, USML will allow flight of a larger number of devices than a GAS can allow, and permit easier monitoring of operational parameters. Timelines and some materials will be fully defined in 1989-91, so the descriptions that follow are preliminary:

1. Non-linear optical organic crystals uses 40 quartz ampoules in 20 organic transport ovens similar to those in GAS 105. Each oven con-

tains two quartz ampoules enclosed by aluminum tubes, one nested in the other. To reduce heat transfer, the outside of the outer tube and the inside of the inner tube are coated with gold, the void between the tubes is evacuated and a special polymide packing is used as a spacer to position the ampoules inside the inner tubes. Each oven is 13.7 inches long and 4.1 inches wide, and weighs only 4.4 pounds (Figure 4-1).

2. Non-linear optical monomer thin films uses an apparatus identical

ORIGINAL PAGE IS
OF POOR QUALITY

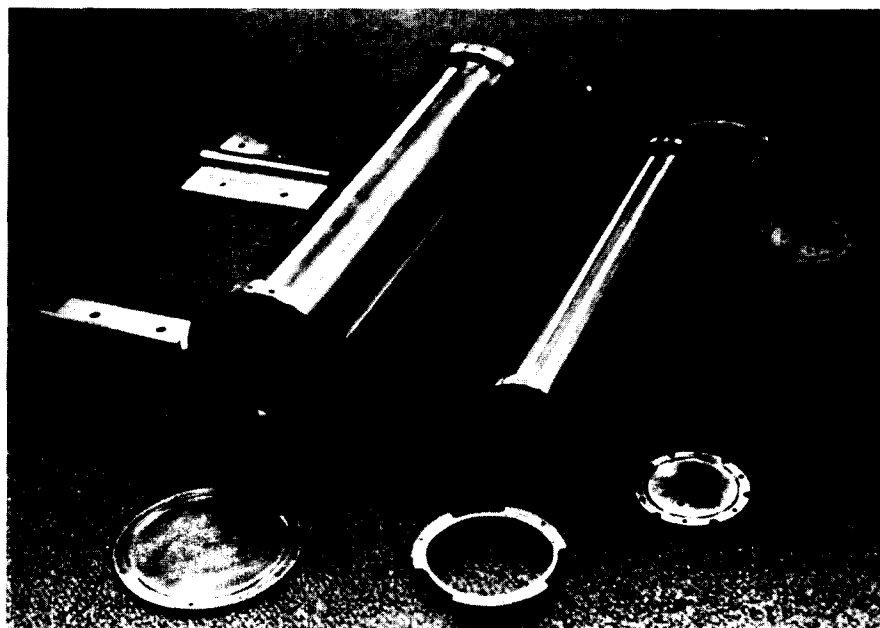


Figure 4-1
Major elements of standard vapor transport oven designed by CMDS

for GAS 105 and USML (above) and assembled unit on mounting rails (below).



to the one described above.

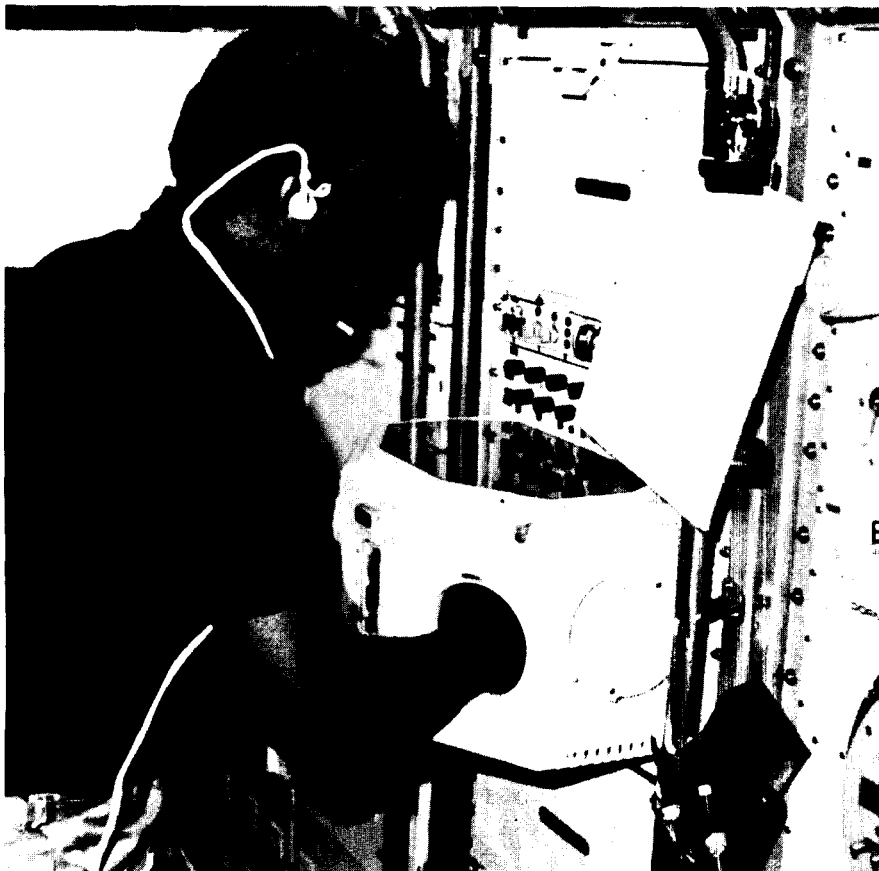
3. Electrodeposition uses a set of 20 to 30 2-inch cubic cells mounted to a base plate. Most of the cells will be used for electrodeposition of positive metal ions from a liquid solution or codeposition of dense, hard neutral particles and metals. Two or three will be used to electroform crystalline materials. These processes, and LED readouts of electrical and thermal conditions, will be photographed with video and 35mm film cameras.
4. Organic separation experiment is a modified version of the phase partitioning experiments carried out with handheld and automated devices. Each of 10 cells will have a rotating disk in the upper section. The top part of the cell is coated to attract one phase and the bottom part is coated to attract the other. During the experiment the top part of the cell is

rotated to shear the the two phases apart for repeated applications of the process. Polymers, live cells, and other materials will be installed in the sample cells. Temperatures will not be allowed to exceed 30°C to protect the cells. Before and after the experiment the cells will be cooled to 4°C.

5. Elastomer modified epoxy resins will use an oven apparatus similar to that of the organic crystal experiments described in (1) and (2).
6. Foam formation experiment may be conducted inside the Materials Science Glovebox (Figure 4-2). The components will be mixed by a stirring mechanism as plungers push them out of their respective tubes. Upon mixing the the foam formation process begins; this will be photographed by 35mm cameras. When complete the foam, which now fills about a 10-inch cube, is removed and placed in the air to cure before storage.

Figure 4-2

Mission Specialist Guion Bluford performs an experiment within the confines of a glovebox during the Spacelab D-1 mission.



ORIGINAL PAGE
BLACK AND WHITE PHOTOGRAPH

Project: Surface Coatings and Catalyst Production by Electrodeposition

Industrial Participant: George Maybee, McDonnell Douglas Astronautics Company-Huntsville, 689 Discovery Drive, Huntsville, AL 35806.

UAH: Clyde Riley, Department of Chemistry

Introduction

This project is concerned with the study of electrodeposition and electrocodeposition and applications of these processes. As a result of these efforts we would hope for a better understanding of (a) the role of convection and buoyancy in the mechanisms for formation of some electrodeposited surfaces, (b) the effect of electrodeposition rates coupled with low-g upon depositing surface morphology, (c) concentration gradients in the vicinity of electrodepositing surfaces, (d) the effect of gravity upon the dispersion (coagulation) of neutral particles that are codepositing, (e) the influence of (lack of) a moving medium upon codeposition, (f) preparation of improved surface coatings and metal catalysts.

Background

Simple Electrodeposition: In this study we are concerned only with cathode reduction of metal ions from aqueous solution is shown in Equation 5.1-1 where M^{n+} is a solvated metal cation with formal charge, n^+ ; e^- denote an electron and $m(s)$ represents reduced metal atoms depositing at the cathode. Assuming a one dimension process (ion diffusion toward the cathode) the ion concentration gradient in the vicinity of a diffusion controlled electrode should follow Fick's second law.

In Equation 5.1-2 where $C(x,t)$ represents the time variation of cation concentration C in a plane parallel to a flat electrode at a distance x , and D is the diffusion coefficient for the cation; $C(x,t)$ can be determined by

integration or by numerical difference techniques. The latter readily allows one to include the concentration dependence of diffusion coefficients. Equation 5.1-2 also leads to the instantaneous current^{1,2}. In equation 5.1-3, F is the Faraday constant, A is the electrode area and C_0 is the bulk cation concentration in the cell.

Codeposition: Several mathematical models have been formulated for the treatment of electrocodeposition. Gugliemi applies a modified Langmuir adsorption isotherm utilizing a two step process for occlusion of the neutrals (cermets) within the forming metal matrix³. Particles are initially loosely adsorbed on the surface and are treated as being in equilibrium with those in suspension. This treatment assumes homogeneous suspension and ionic concentrations of C_m and C_0 respectively, resulting in a working Equation (5.1-4), where α is the volume fraction of particles in the deposit, W is the atomic weight of the depositing metal, F is Faraday's constant, n the number of electrons required to reduce the cation to an atom, d the metal density, $\nu \exp^{B\eta}$ is an exponential rate factor for strong adsorption in which ν is the overpotential and ν_0 , A and B are adjustable parameters, i_0 is the exchange current, and k is the ratio of rate constants for adsorption and desorption which depends upon the intensity of interaction of the particles and the electrode.

Celis, Roos and Buelens recently formulated a model for electrocodeposition which addresses some of the shortcomings of earlier models including that of Gugliemi⁴. They assume a five-step mechanism for the inert particle on its way from the bulk of solution to the site of incorporation in the depositing metal matrix at the cathode: (a) adsorption of ionic species upon the particle surface; (b) movement of the particle by forced convection towards the hydrodynamic boundary layer; (c) diffusion of the particle through the diffusion

5

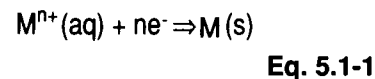
Individual Projects

5.1

Surface coatings & catalyst production

Table 5.1

Electrodeposition equations



$$\frac{dC(x,t)}{dt} = D \frac{d^2C}{dx^2} \quad \text{Eq. 5.1-2}$$

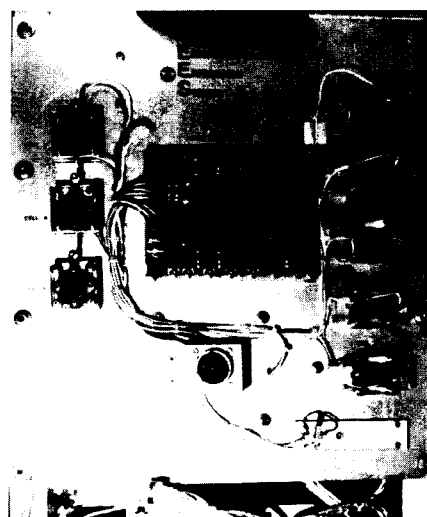
$$i_t = \frac{n F A D^{1/2} C_0}{\pi^{1/2} t^{1/2}} \quad \text{Eq. 5.1-3}$$

$$\frac{C_m}{\alpha} = \frac{W i_0}{n F d v_0} \exp^{(A-B)\eta} \left[\frac{1}{k} + C_m \right] \quad \text{Eq. 5.1-4}$$

$$W/O = \frac{100 W_p N_p P}{\frac{M_i}{nF} + W_p N_p P} \quad \text{Eq. 5.1.5}$$

Figure 5.1-1

Electrodeposition apparatus with five cells at right and three at left.



ORIGINAL PAGE IS
OF POOR QUALITY

ORIGINAL PAGE BLACK AND WHITE PHOTOGRAPH

Figure 5.1-2
Codeposition cells mounted before 35mm camera.

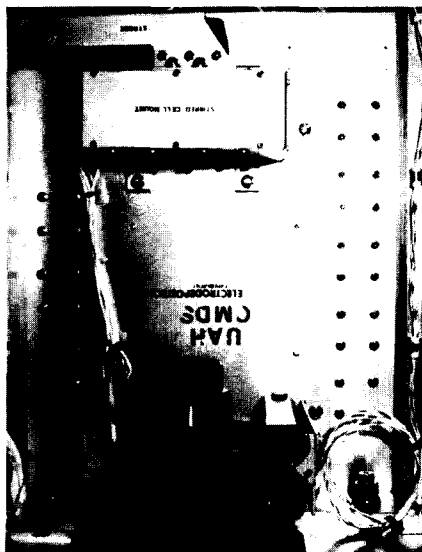
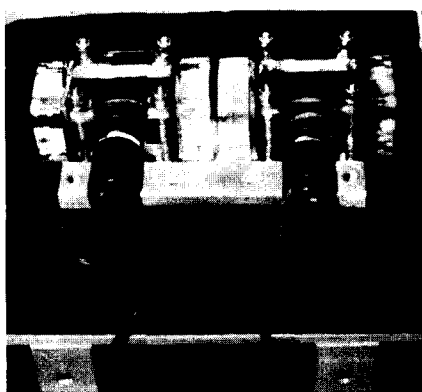


Figure 5.1-3
Rear view of codeposition cells showing motor drives for stirrers.



double layer; (d) adsorption of the particle, still with its adsorbed ions, at the cathode surface; (e) reduction of some adsorbed ions resulting in the particle's irreversible incorporation in the depositing metal matrix. This model leads to equation 5.1-5 where W/O is the weight percent of embedded particles, W_p is the mass of one particle, N_p is the number of particles crossing the diffusion layer per unit time and unit surface area, P is the probability of incorporation in the cathode, M is the atomic weight of the depositing metal; i is the current density and F is the Faraday constant. P has been formulated statistically and N_p is related to bulk particle/ion concentrations.

Both (4) and (5) assume a homogeneous suspension of particles by convective stirring. If the system is not stirred in low-g, gradients for the particles as well as ions would occur and thus (4) and (5) would not be applicable after a short time.

Experimental work

A spatially resolving absorption spectrophotometer has been completed. Figures 5.1-4 and 5 show the optical and electronic components of the apparatus. The electronics of Figure 5.1-4 comprise an AT computer, array controller and cell potentiostat. The optics of Figure 5.1-5 from right to left includes a 4 mw diode laser (814 nm), cell and mount, lens and mirror. Reflection is then back to the lower right mirror and subsequent projection on the array which is visible in the lower left corner of Figure 5.1-5. Total light filters and a wavelength specific filter protect the front of the array. All are mounted on an optical track which is secured to an aluminum slab and enclosed in a dark box. The container and slab was bolted to the KC-135 deck.

Design and Fabrication: Much of 1987-88 was dedicated to the design and construction of a flight apparatus for a sounding rocket. The 10-cell

apparatus is pictured in Figures 5.1-1 through 5.1-3. Figure 5.1-1 shows the electrodeposition side of the board with eight cells. At least seven of these cells will contain nickel sulfamate and the eighth will contain nickel sulfamate or cobalt sulfate. The five cells on the right are the "regular" cells with electrodes at 3.8 cm spacing. They have been altered to compensate for pressure build-up by the insertion of sealed compressible rubber tubing in a machined slot on the side of the cell cavity. This was necessary since these cells would be operated at high voltages to give high rates of nickel deposition and thus would also produce gas from H_2O electrolysis. The cells on the left have short electrode spacings of 0.95cm to reduce the ohmic overpotential. These cells can be run at high rates at low voltage but with minimal H_2O electrolysis. The cathode areas in the shortened cells will be varied by masking to give several different electrodeposition rates. The electronics board in the center of Figure 5.1-1 is linked with the flight central processor. Cell currents and the temperature in a central location will be recorded intermittently. Figure 5.2-2 shows the back side of the apparatus. The camera is focused on the stirred cell mount which contains the codeposition cells that are exposed more clearly in Figure 5.1-3.

One stirred cell contains cobalt sulfate and chromium carbide and the other nickel sulfamate and diamond dust. Stirring is accomplished with an internal bar and an external magnet rotated by a gear motor. The gear motor's lower turning speed assures coupling between the rotating magnet and internal bar which must be assumed will be resting against the magnetic cobalt or nickel anode in each cell after launch.

The entire apparatus has passed a rigid vibration test performed by Wyle Laboratories of Huntsville.

ORIGINAL PAGE IS OF POOR QUALITY

Results and conclusions

Oscillatory Cell: We are attempting to model this process in cooperation with Daniel Thomas, Assistant Professor of Chemical Engineering (UAH). Differential equations for a porous film in a hydrodynamic flow have been formulated. It is thought that shaking the cell results in; (a) uncovering a porous portion of the anode (becomes conducting); (b) establishing a flow pattern in the cell which is damped very slowly (hours). It is to be noted that although we return the cell to a non-convecting anode operation, the flow pattern imprinted by shaking is still retained. This gives rise to oscillations that are many minutes apart and of several minutes duration as the unsaturated fluid traverses the anode surface in its flow pattern. As the flow dampens with time, as expected, the oscillatory period not only increases, but the amplitude of the oscillation becomes longer.

Codeposition: No further work was done on particle coagulation this past year. Before we pursue this any further we would need to quantify the coagulation. This would require a sizing apparatus which works in low-g and in less than 25 seconds. No commercial apparatus exists that can provide data under these conditions. A cell, microscope, video camera and a digitizer would be necessary to measure particle sizes under these conditions.

Catalyst Preparation: We outlined our KC-135 work and its comparison to that of Erhardt's TEXUS Program results⁵⁻⁸ in last year's report⁹. Our rocket flight apparatus is essentially dedicated to the reproduction of the TEXUS Program results. Amorphous materials offer many advantages as heterogeneous catalyses¹⁰. Among these are single phase, isotropy and highly reactive surfaces.

We are also studying the possibility of atom cluster formation in low gravity. Planar amorphous surfaces that could be anodized and subse-

quently have their pores "loaded" with active metal clusters could offer many possibilities.

Concentration Gradients by Spatially Resolving Spectrophotometry: The spatial spectrometer has been constructed. It has passed a NASA readiness inspection for KC-135 and has been manifested. We shall process copper solution in our shake-down flight. If all goes well we will borrow or purchase a small argon ion laser (or possibly use a broadband LED/filter arrangement) to process cobalt solution.

References

1. C. Riley, D. Coble and G. Maybee, "Electrodeposition of Metals and Metal/Cermet Composites in Low Gravity," AIAA-87-0510, Reno, Nevada.
2. Ralph N. Adams, *Electrochemistry, At Solid Surfaces*, Marcel Dekker, Inc. New York, (1969), Chap. 3.
3. N. Gugliemi, *J. Electrochem. Soc.*, 119, 1009 (1972).
4. J. P. Celis, J. R. Roos, and C. Buelens, *J. Electrochem. Soc.*, 134, 1402 (1987).
5. Josef Ehrhardt, "Dispersion Electrolysis Under Zero Gravity in the SPACELAB Program TEXUS IV." Battelle-Institute, BMFT Reference No. 01 QV 219-AK-SN/A-SLN 7910-5. April 1982,
6. J., "TEXUS VII." BMFT Reference No. 01 QA 219AK- SN/A-SLN 7910-5, November 1983 and

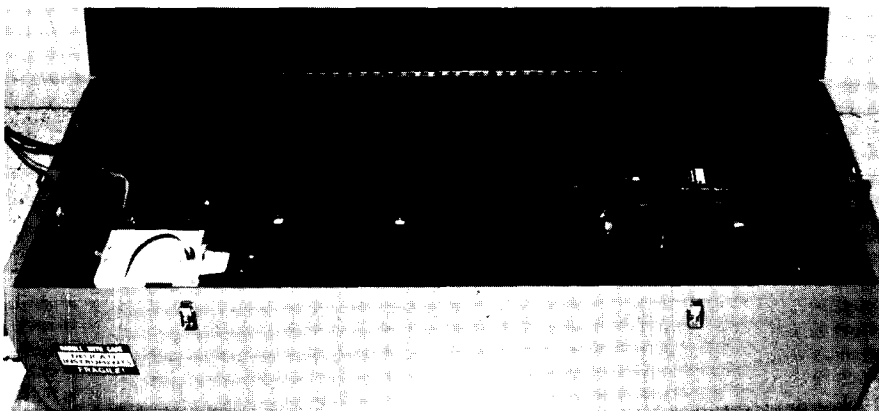
Figure 5.1-4

AT computer and interface equipment mounted in rack for flight aboard KC-135.



Figure 5.1-5

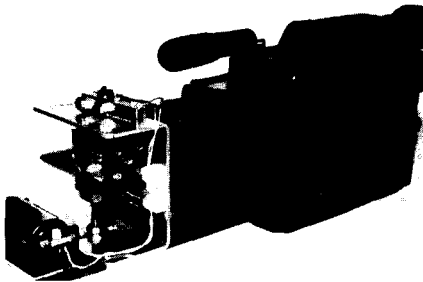
Arrangement of spectrophotometer flown aboard KC-135.



ORIGINAL PAGE
BLACK AND WHITE PHOTOGRAPH

Figure 5.1-6

Camera and electrodeposition cell arranged for KC-135 flight as shown on cover of this report.



5.1.1 Measurement of diffusion coefficients

7. "TEXUS IX." BMFT Reference No. 01 QV 014-AK/SN, November 1984.
8. J. Ehrhardt, *Galvanotechnik*, D 7968, Sauligan 72. 13 (1981).
9. Clyde Riley, H. Dwain Coble, Boon H. Loo, "Surface Coatings and Catalyst Production by Electrodeposition." Annual Report, Consortium for Materials Development in Space, NAGW-812 September 1987.
10. David L. Cocke, *Journal of Metals*, February, 70 (1986).

Presentations and publications

1. G. Maybee, C. Riley and D. Coble, "Microgravity Effects on Electrodeposition of Metals and Metal Cermet Mixtures," GAS Conference, October 1986, Goddard Space Flight Center, Greenbelt, MD.
2. C. Riley, D. Coble and G. Maybee, "Electrodeposition of Metals and Metal/Cermet Composites in Low Gravity," AIAA-87-0510, Reno, Nevada
3. B. H. Loo, C. Riley, H. D. Coble and H. Abi-Akar, "Oscillatory Behavior of Cobalt," Alabama Academy of Science meeting, Florence, AL, March 1987.
4. C. Riley, H. D. Coble, B. Loo, B. Benson, H. Abi-Akar, and G. Maybee, "Electrodeposition and Codeposition Under Low Gravity/Nonconvecting Conditions," *Polymer Preprints*, 2, 470 (1987).
5. C. Riley, H. D. Coble, B. Loo, B. Benson, B. Abi-Akar and G. Maybee, "Electrode Position and Codeposition Under Low Gravity/Nonconvecting Conditions". (Invited presentation, 194th ACS National Meeting, New Orleans, LA, September 1987.)
6. Brian Benson and Clyde Riley, "Determination of Concentration Gradients During Electrodeposition Under Low G Conditions Using Spatially Resolved Spectrophotometry" (Submitted for AIAA-89, Reno, Nevada).
7. Clyde Riley, Hind Abi-Akar, Brian Benson and George Maybee, "Electrodeposition of Metals and Metal/Cermet Composites on a Sub-Orbital Rocket" (Submitted for AIAA-89, Reno, Nevada).

Subproject: Measurement of Diffusion Coefficients Using the Diaphragm Cell

UAH: James K. Baird

Introduction

This year's effort involved experimental tests and theoretical extensions of the equations derived last year. In addition to the cell whose calibration was started last year, we have constructed and calibrated three additional cells. As the characteristic diffusion time in most cells is 7-8 days, the rate of data acquisition with any one cell is necessarily slow. We are thus routinely running all four cells continuously in order to gather data more rapidly.

To test our theory of the measurement of concentration dependent diffusion coefficients, we chose an

aqueous solution of sucrose at 25°C. The diffusion coefficient of this solution is known to be a strong function of concentration, providing presumably optimal conditions for measuring the higher order terms in our theory. At a sucrose concentration of 0.05 M, we found the diffusion coefficient to be 5.3×10^{-6} cm²/sec in good agreement with previous measurements, but there was no evidence for the existence of the higher order corrections in our theory. Since the largest of the correction terms for which we were searching was second order, we concluded that it must have been too small for detection given our experimental error. Because the diffusion coefficient of aqueous sucrose is low, these experiments also proved to be quite slow.

Our experience with sucrose lead us to generalize our theory to take into account the case where the volumes above and below the sintered glass disk are different. In this case, the correction terms are larger, and the diffusion time, t , is related to the concentration difference, Δc , across the frit (Equation 5.1.1-1).

Here $c_1(t)$ and $c_2(t)$ are the solute concentrations below and above the frit, respectively. The coefficient, B_L , is given by Equation 5.1.1-3 where β is the cell constant and $D(\bar{c})$ is the diffusion coefficient evaluated at the mean concentration, \bar{c} , as given in Equation 5.1.1-4, which is a constant of the motion. The volumes below and above the frit are V_1 and V_2 , respectively.

The next coefficient in Equation 5.1.1-2 is given by equation 5.1.1-5 where $D^{(1)}(\bar{c})$ is the first derivative of $D(\bar{c})$ with respect to c evaluated at $c = \bar{c}$. If $V_1 = V_2$, all odd order coefficients are zero, and Equation 5.1.1-1 conforms to the result reported last year.

We note that if $c_1(0)$ and $c_2(0)$ are properly adjusted, the mean concentration can be left the same while V_1 and V_2 are varied. In this way, we are assured that B_L is invariant, while the magnitude and sign of B_1 depends upon V_1 and V_2 . This scheme provides a nice test of Equations 5.1.1-1 through -5. We have carried out this experiment using aqueous hydrochloric acid, where the diffusion is an order of magnitude faster than with aqueous sucrose. We found that, although B_L is the coefficient of a first order correction, its effect (and that of all higher order terms) on Equation 5.1.1-1 is still quite small. The precision of our data was sufficient to observe the sign change predicted by Equation 5.1.1-4 but insufficient to specify its magnitude very accurately.

On the basis of the experiments with sucrose and with hydrochloric acid, we have concluded that the higher order terms in Equation 5.1.1-

1 can be safely ignored. The first two terms alone are sufficient to analyze data and to determine $D(\bar{c})$.

We have proceeded in this fashion to determine the concentration dependence of the diffusion coefficient of aqueous copper sulfate, a solution to be used in the electrodeposition

Table 5.1.1-1

Equations of diffusion

$$\Delta c = c_1(t) - c_2(t)$$

Eq. 5.1.1-1

$$t = B_0 + B_L \ln(\Delta C) + B_1(\Delta C) + B_2(\Delta C)^2 + B_3(\Delta C)^3 + \dots$$

Eq. 5.1.1-2

$$B_L = \frac{-1}{\beta D(\bar{c})}$$

Eq. 5.1.1-3

$$\bar{c} = \frac{C_1(0)V_1 + C_2(0)V_2}{V_1 + V_2} = \frac{C_1(t)V_1 + C_2(t)V_2}{V_1 + V_2}$$

Eq. 5.1.1-4

$$B_1 = \frac{D^{(1)}(\bar{c})}{2\beta(D(\bar{c}))^2} = \frac{V_2 - V_1}{V_2 + V_1}$$

Eq. 5.1.1-5

experiments. Table 5.1.1-2 summarizes our results. Between 0.125 M and 0.875 M, the diffusion coefficient of this system varies by more than a factor of two. At the higher concentrations, the diffusion coefficient is less than 10^{-5} cm²/sec, which is typical behavior for most salts containing the sulfate anion. Experiments are currently under way to extend this data to both lower and higher concentrations. Additional experiments have been started to measure the diffusion coefficients of aqueous cobalt sulfate and nickel sulfamate, both of which are to be used in the electrodeposition experiments.

Table 5.1.1-2

D(c) for aqueous copper sulfate at 25°C	
c(M)	D(c) (10⁻⁵cm²/sec)
0.125	1.170
0.250	0.793
0.375	0.673
0.500	0.544
0.605	0.440
0.750	0.431
0.875	0.488

ORIGINAL PAGE
BLACK AND WHITE PHOTOGRAPH

5.2 Physical vapor transport crystal growth

Project: Physical Vapor Transport
Crystal Growth

Industrial Participant: Victor
Sweberg, Boeing Aerospace Co.,
Seattle, WA 98124

UAH: Elmer Anderson, H. Y. Cheng,
Department of Physics

grow at lower temperatures, (3) characterization of the crystals grown on the project and (4) development of requirements for the flight system. The past year's efforts toward achieving these goals are summarized below.

Introduction

Single crystals of zinc selenide have numerous applications in optical devices¹ and consequently there is a demand for crystals of greater optical quality for use in p-n junction light-emitting diodes²⁻⁶, laser windows, gradient index materials, photoconductors, etc. When doped with sulphur, the compound $ZnS_{1-x}Se_x$ is a blue emission material. Growth has been achieved under moderate pressure from the melt as well as from chemical and physical vapor deposition, and thin films have been made by evaporation and by epitaxial growth. The growth method used in this study is that of vapor transport and condensation within a sealed quartz ampoule. Physical vapor transport has the advantage of requiring lower temperatures than growth from the melt and it is less vulnerable to the severe strains that can result from growth at very high temperatures. Physical vapor transport is less complex than growth by chemical vapor transport since the latter method often involves a number of different molecular species, all of whose vapor pressures must be known as a function of temperature.

Boeing Aerospace Company and CMDS expect to fly a joint experiment on the growth of zinc selenide or similar materials after Space Shuttle flights resume. In support of the flight system development program, investigators at BAC and UAH are currently concentrating their efforts upon the following ground-based activities: (1) determination of the optimum growth conditions for zinc selenide, (2) consideration of alternative crystals which

Crystal growth

Last year's Annual Report summarized our procedures for pre-treating the starting materials, preparing the ampoules, and growing the boules. The factors affecting the transport of material and the nucleation of growth at the desired site were also discussed in that report and elsewhere.^{7,8}

Growth data for nine runs are given in Table 5.2-1. Although the initial growth of each of these boules was polycrystalline as the boule emerged from the cavity in the cold finger, some of these crystallites developed to sizes of 4 or 5 mm as the boules grew. The average growth rate of each boule was determined by simply dividing the weight of the boule by the total length of the growth run. This number represents a lower limit since it is not known at what time during the run all transport ceased. Using the above method, the largest growth rate obtained was 280 mg/day for boule number 16. This corresponds to an average transport rate of about 10^{-8} moles/cm²/sec or 1.93×10^{-3} moles/day. This compares favorably with the growth rate of about 1 millimole per day reported by Fujita et al.⁹ The maximum growth rate has not yet been determined since the growth rate achieved in the laboratory is so dependent upon the rate at which the ampoule moves through the thermal gradient. A linear growth rate of 0.5 mm/day was reported by Huang and Igaki¹⁰, while our highest linear rate is estimated to be greater than 1 mm/day for run number 16. Our average pull rate was about 1 mm/day. We plan to study this problem further using a traveling

Figure 5.2-1
Grow steps in boule 3 (x320).

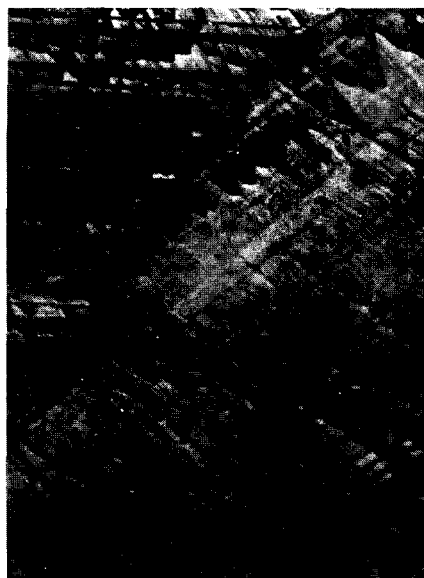


Table 5.2-1

ZnSe growth rates			
Run No.	Run Time (days)	Material Xport. (grams)	Avg. Growth (mg/day)
2	10	1.44	144
3	15	2.52	168
4	20	2.04	102
5	22	0.50	23
6	32	3.44	100
8	20	2.23	112
9	23	3.01	131
13	13	5.45	176
16	9	2.52	280

furnace with a drive mechanism which can provide as little as 0.5 mm of linear movement/day. It should be kept in mind that the optimum growth rate is not necessarily the fastest rate, but it is the highest rate consistent with good crystal quality. Therefore an active program of crystal characterization must accompany the study of growth rates.

Crystal characterization

The following techniques are employed in evaluating the quality of the boules grown. First, the boules are examined under optical microscopes and photographed. Next they are sliced into wafers having a thickness of 1 or 2 mm and these are examined for their structural homogeneity and compositional purity using optical microscopy, x-ray diffraction, and electron microprobe analysis. No crystal structures other than the ZnSe structure have been detected. The only impurities detected by characteristic x-ray analysis were slight traces of calcium and sulfur, although these have not shown up for all samples. Wafer surfaces are then polished with a final grit size of 0.25 μm and then scanned at high magnification using the scanning electron microscope (SEM) and the Raman microprobe. Video tapes have been made of some of the optical microscope scans. The polished wafers are also examined with the SEM. The wafers are then etched in a 10% solution of bromine in methyl alcohol for 1 or 2 minutes and again viewed in the SEM and the Raman microprobe. Some typical results are shown below.

Figure 5.2-1 is a view of growth steps in two grains of boule 3 after etching, taken with an optical microscope (320x). Figure 5.2-2 is an electron micrograph (800x) of dislocation etch pits in boule 3. The distorted triangular shape of the pits indicates that the (111) planes are tilted with respect to the surface of the photo. An example of twinning is

shown in Figure 5.2-3 which is an electron micrograph (320x) of a section from boule 5. A grain boundary in boule 13 is shown in Figure 5.2-4 enlarged 320x. Figure 5.2-5 shows dislocation etch pits (800x) in boule 13. Here the etch pit density is about $106/\text{cm}^2$, which is about 100 times greater than desirable. This could indicate that the boule was under unusually large thermal stress during growth or during the cool down.

References

1. Oliver, D. S. and W. R. Buchan, *IEEE Trans. Electron Devices* ED-18, 769 (1971).
2. Allen, J. W., A. W. Livingstone and K. Turvey, *Solid State Electron.* 15, 1363 (1972).
3. Ozsan, M. E. and J. Woods, *Appl. Phys. Letters* 25, 489 (1974).
4. Ozsan, M. E. and J. Woods, *Solid State Electron.* 18, 519 (1975).
5. Ozsan, M. E. and J. Woods, *J. Phys. D* 10, 1335 (1977).
6. Lawther, C. and J. Woods, *Phys. Stat. Solidi* 50a, 491 (1978).
7. Cheng, H. Y., E. E. Anderson and M. K. Wu, *Bull. Amer. Phys. Soc.* 32, 610 (1987).
8. Cheng, H. Y. and E. E. Anderson, *Bull. Amer. Phys. Soc.* 33, 742 (1988).
9. Fujita, S., H. Mimoto, H. Takebe and T. Noguchi, *J. Crystal Growth* 47, 326 (1979).
10. Huang, X. N. and K. Igaki, *J. Crystal Growth* 78, 24 (1986).

Presentations and publications

Anderson, Elmer E., and Hai-Yuin Cheng, "Growth of ZnSe Crystals by PVT." Alabama Materials Research Conference, Sept. 29-30, 1987, Birmingham, AL.

Cheng, Hai-Yuin and Elmer E. Anderson, "Growth of Centimeter Size ZnSe Single Crystals by PVT." *Bull. Amer. Phys. Soc.* 33, 742 (1988). Paper presented at the New Orleans APS meeting, March 21-25, 1988.

Figure 5.2-2

Dislocation etch pits in boule 3 (800x).

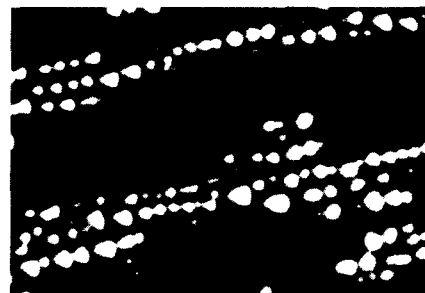


Figure 5.2-3

Twinning in boule 95 (320x).



Figure 5.2-4

A grain boundary in boule 13 (320x).



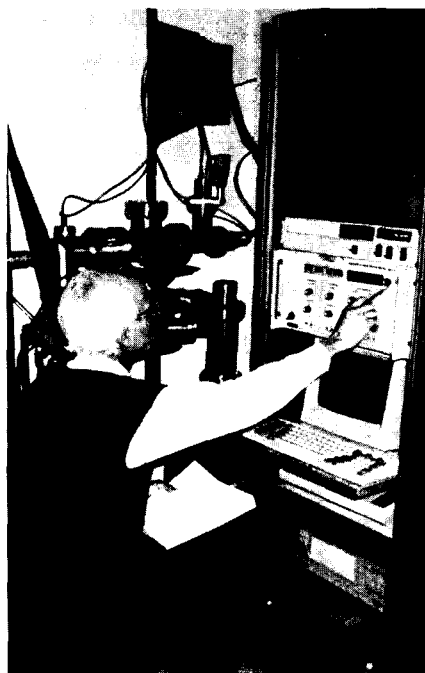
Figure 5.2-5

Dislocation etch pits (800x) in boule 13.



5.2.1 Mass spectroscopic facility

Figure 5.2.1-1
Rosenberger operates the CMDS-CMMR joint mass spectroscopic facility.



Subproject: Mass Spectroscopic Facility

UAH: Franz Rosenberger, Center for Microgravity and Materials Research

Introduction

Both the CMDS and the Center for Microgravity and Materials Research (CMMR) are pursuing projects that will greatly benefit from an in-house chemical characterization of materials at high temperatures. Since CMMR personnel has experience with the mass spectroscopy of high temperature vapors, it was decided to establish a joint mass spectroscopic facility.

A mass spectrometer system was designed based upon:

- Balzer's QMG 511 quadrupole mass spectrometer (mass range 2-1023, cross beam ion source with electron acceleration voltage adjustable 5-120V),
- Balzer's TSU 170 turbomolecular pump station (170 liters/sec),
- Alcatel 37-63M/E2M2G diffusion pumping system (for evacuation of [dirty] sample furnace space), and
- Teknivent Vector/One mass spectrometer computer for control and data acquisition.

During the report period, these core components were functionally connected via a system of ultra-high

vacuum components, valves and vacuum gauges, that will allow for an efficient operation and rapid sample exchange. Furthermore, we have designed, in interaction with Vacuum Generators, Ltd. and EPI Systems, a novel high temperature effusion cell mounted on a linear motion device that will facilitate the positioning of the molecular beam source in close proximity of the ionization region of the mass spectrometer. Orders for these components have been placed and their integration into the system can be expected by early 1989.

The remaining task for the completion of the mass spectroscopic facility consist of the design and construction of a cryogenic collimator that minimizes the formation of molecular species that are sample-non-specific.

The first investigations to be conducted with the completed facility will be concerned with the high-temperature out-gassing behavior of quartz ampoules and the vapor composition in crystal growth experiments of the CMDS. These will give important insight on the prevailing transport mechanisms in these crystal growth experiments and supply a realistic basis for the numerical modeling of heat and mass transfer in these systems.

ORIGINAL PAGE
BLACK AND WHITE PHOTOGRAPH

ORIGINAL PAGE BLACK AND WHITE PHOTOGRAPH

coworkers in this area. We now have in hand some "tub-shaped" cylinders, which we have coated to provide varying contact angles between the phases and the walls. These containers will be flown on the KC-135 to get a preliminary indication of the power of this approach.

Extension of affinity phase partitioning

A major interest of ours is in developing the technique of affinity phase partitioning (with polymer two-phase systems) for eventual use in low-g separation of cells of commer-

In our most recent work in this area we have applied the affinity partitioning technique to protein purification. Protein purification is now a major limiting factor in applying recombinant DNA technology to prepare important proteins. In our procedure we have attached an antibody to the enzyme alkaline phosphatase to PEG. When the PEG-antibody is included in a dextran-PEG two phase system, the enzyme is pulled into the top, PEG-rich phase, and all other proteins are left in the bottom, dextran-rich phase. We will publish this work soon.

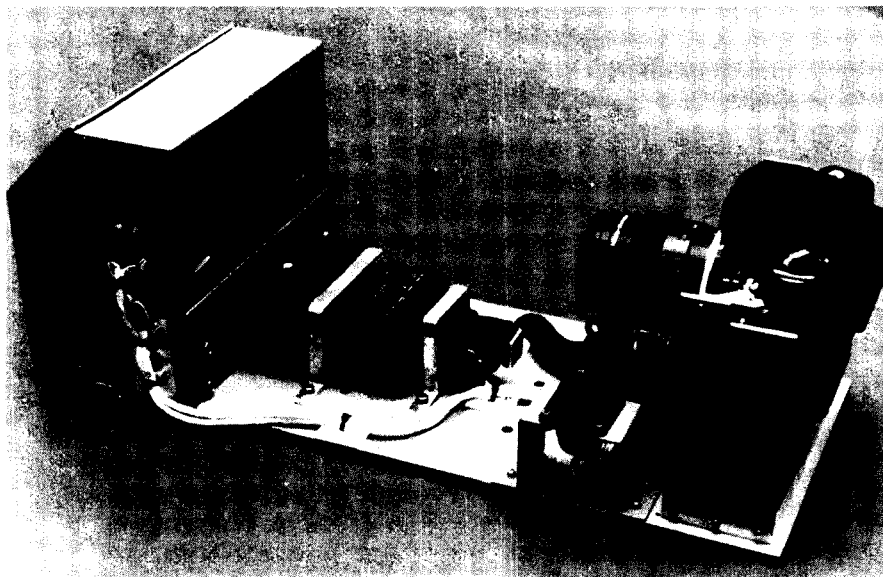
Refinement of chemistry

The polymer coating work and the affinity partitioning procedure requires a great deal of chemistry which is in constant need of improvement. In the area of coating chemistry, we have spent a great deal of time optimizing the first step, which is aminating glass with triethoxy-aminopropyl silane. Although this reaction has been used for several years now, it continues to cause problems. Our recent work has been aided by the availability in the Surface Science Center of an X-ray photoelectron spectrometer to analyze the aminated surfaces. In addition we are now examining use of polyethylene imine for laying down a surface amine layer.

In the PEG-protein area, we have developed a new PEG activation procedure based on PEG tresylate rather than the much-used PEG cyanuric chloride activation. This procedure gives more active protein.

Finally, we have extensive results on anion-initiated polymerization of ethylene oxide to produce novel PEGs. This polymerization provides us with control over polymer molecular weight and end groups. Previously we were restricted to commercial materials.

Figure 5.4-2
Complete demixing apparatus assembled for flight.



cial importance. Previous work has shown that gravity-driven demixing of the polymer two-phase systems greatly reduces the efficiency of phase partitioning on Earth; if this randomizing force were removed from affinity phase partitioning, a cell separation procedure of perfect selectivity (no undesired cells would be retained) would be provided. Affinity phase partitioning, previously developed by us, utilizes an affinity ligand (an antibody) covalently attached to PEG to pull cells into the PEG-rich phase (unwanted cells remain at the interface between the PEG-rich and dextran-rich phases).

Publications and presentations

Bamberger, S.B., J. M. Van Alstine, J. M. Baird, J. M. Harris, and D. E. Brooks, "Demixing of Aqueous Polymer Two-Phase Systems in the Absence of Gravity," *Sep. Sci. Tech.*, 23, 17-34 (1988).

Harris, J.M., D. E. Brooks, J. F. Boyce, R. S. Snyder, and J. M. Van Alstine, "Hydrophilic Polymer Coatings for Control of Electroosmosis and Wetting," in *Dynamic Aspects of Polymer Surfaces*, J. D. Andrade, Ed., Plenum, 1988, pp 111-119.

Karr, L.J., J. M. Van Alstine, R. S. Snyder, S. G. Shafer, and J. M. Harris, "Cell separation by immunoaffinity phase partitioning with PEG-modified protein A," *J. Chrom.*, 442, 219-227 (1988).

Harris, J.M., K. Yoshinaga, M. S. Paley, and M. R. Herati, "New Activated PEG Derivatives for Affinity Partitioning," *Advances in Separations Using Aqueous Phase Systems in Cell Biology and Biotechnology*, D. Fisher and I. A. Sutherland, Eds., Plenum, London, 1988, in press.

Project: Nuclear Track Detectors

Industrial Collaborator: John C. Gregory, Frontier Research, Inc., P.O. Box 1261, Huntsville, AL 35807.

UAH: Samuel P. McManus, Department of Chemistry

Introduction

Passive nuclear track detectors made of polycarbonate materials have become extremely important in the study of cosmic rays. Such materials are also finding use as neutron detectors. Production of materials that have a sensitivity between the commonly use photographic emulsions and CR-39 is of interest to researchers using the detectors to study cosmic rays and is a goal of Frontier Research.

An experiment planned for GAS 105 is a series of passive nuclear track detectors to evaluate the particle background induced in a small emulsion calorimeter. In addition to photographic emulsion particle detectors, plastic materials suitable for measuring several elements will be included. Since the experiment is totally passive, the hardware consists entirely of the container with the enclosed detector materials.

During the past year an effort to prepare a new plastic material, sensitive to elements between lithium and iron, has been carried out. The new molecular design takes into account the way the polycarbonate molecules are cleaved by high energy cosmic ray particles. This program will continue with the goal of including this material with the GAS-105 experiment.

5.5 Nuclear track detectors

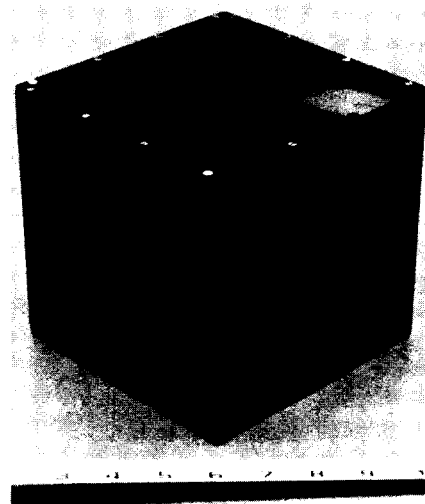


Figure 5.5-1
Housing for stack of nuclear track detector materials for flight on GAS 105.

ORIGINAL PAGE
BLACK AND WHITE PHOTOGRAPH

5.6 Materials preparation and longevity in hyperthermal atomic oxygen

Project: Materials Preparation and Longevity in Hyperthermal Atomic Oxygen

Industrial Participants: Lyle E. Bareiss and Gary P. Sjolander, Martin Marietta Denver Aerospace, Box 179/Mail Stop M-0487, Denver, CO 80201

UAH: John C. Gregory, Department of Chemistry

Figure 5.6-1

Theoretical etch profiles (lower cross sections) for several masking configurations (shown schematically on top). The lower cross sections are greatly magnified vertically as occurs in stylus profilometry measurements.

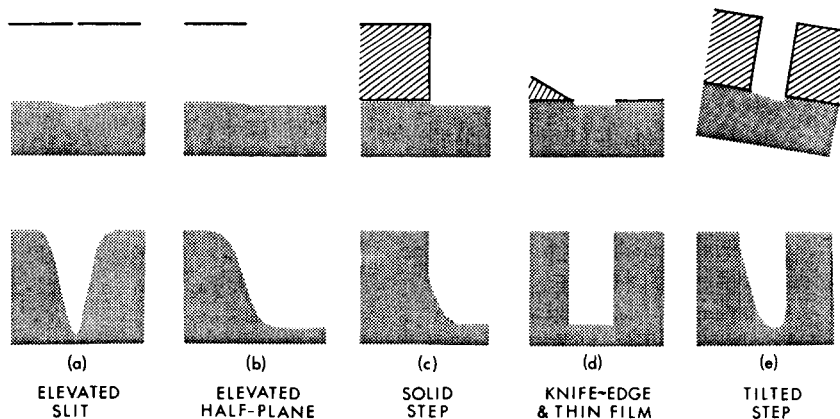
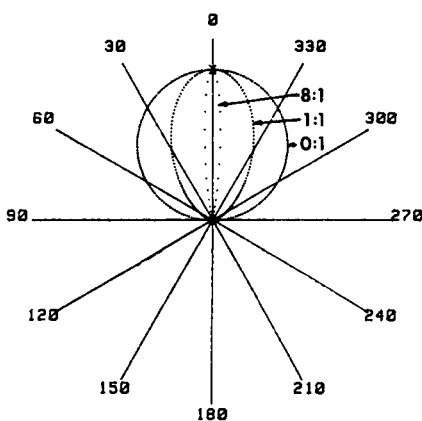


Figure 5.6-2

Calculated angular distributions for atoms (orbital velocity along the 0-180° axis) for three orbital speeds to most probable thermal speed ratios.



Introduction

During the reporting period from October 1987 to September 1988 work was performed on the fabrication of the UAH Atomic Oxygen

Morphology of surfaces etched in orbit

The Maxwell-Boltzmann distribution of speeds of atoms or molecules is asymmetric, but the speeds have random directions so the distribution is spatially symmetric as viewed from a stationary reference frame, and a Gaussian or normal distribution results from examining components parallel to any one axis.

However, relative to a rapidly moving spacecraft (≈ 7.8 km/sec in the thermosphere between 200 and 600 km) the incidence angles of atoms striking surfaces is greatly limited. For forward-facing surfaces the particles are incident within a narrow cone with the flux strongly peaked about normal incidence. The orbital velocity is thus a dominant factor in spaceborne measurements of ambient particles. In this discussion, flux refers to the differential quantity in atoms/cm²/sec, while fluence refers to the flux integrated over time.

Combustible materials, such as carbon and polycarbonate plastics, exhibit heavy etching due to formation of volatile oxides from low activation energy reactions with atomic oxygen in orbit^{2, 3, 4, 6}. The shape of transition or penumbral region of etched surfaces partially shadowed by some object depends both on the thermal speed distribution of the gas and on the spacecraft velocity.

Modeling angular distribution

Nocilla⁵ has considered the case of a moving ensemble of gas molecules. The angular distribution of a beam of gases scattered from a surface was determined by combining the thermal speeds of the particles with their ensemble velocity. Forward-facing surfaces on an orbiting spacecraft experience the equivalent of a high velocity beam incident on exposed areas. To combine the thermal speeds with the orbital velocity we have adapted Nocilla's method with the modification that gases passed

Beam System and on a detailed analysis of the molecular dynamics of oxygen atoms striking a spacecraft surface in low Earth orbit. The vector analysis was shown to be capable of detailed description of the morphology of the roughened surface frequently observed when etchable material surfaces are exposed in space. Such analysis may be used to predict the shapes of surface structures which might be produced in space or in terrestrial beam systems under different experimental conditions. Surface spikes, for example, could be made with a wide variety of aspect ratios to improve some surface-related property such as adhesion, and optical and electrical emissivity or absorptance.

through differential areas rather than scattered from them. An important parameter in the Nocilla model is the ratio of the translational speed of the "mass" (or ensemble) to the most probable speed. Our analagous parameter is the ratio of orbital speed to the most probable speed. We varied this parameter by adjusting the temperature.

Experimental technique

On the STS-8 flight of the Space Shuttle a number of surfaces were exposed to the ambient oxygen in orbit as part of a materials evaluation experiment⁸. This flight was particularly suited to the experiment discussed here since during the entire mission 95% of the 3.5×10^{20} atoms/cm² fluence was accumulated with the Orbiter pointing the experiments within 1° of the velocity vector. The vitreous polished carbon disc was mounted on a heated surface which was tilted slightly ($\approx 4^\circ$) with respect to the velocity direction. Its surface was mounted behind a solid aluminum mask that had an effective height (thickness) of 560 μm at a hole exposing the carbon. Other combustible samples, such as CR-39 (a polycarbonate plastic), were mounted behind masks with knife edges essentially in contact with the sample surface and some samples had thin film mask patterns deposited directly on their surfaces.

Surface profiles of the etched area where mask edges existed were measured after the flight with a stylus profilometer (Tencor Instrument's Alpha-Step 200). Theoretical etch profiles for several simple physical configurations of mask and surface were deduced from integrals of angular distribution calculated for oxygen atoms striking an etchable surface partially covered by a mask (Figure 5.6-1). Comparisons of such theoretical profiles to measured etch profiles were used to estimate the average ambient temperature during exposure.

Results

Computer-generated solutions to Nocilla's equations⁵ are presented for three speed ratios (Figure 5.6-2): zero (the imaginary case of a stationary satellite, or an ensemble of gases moving with the satellite); unity (imaginary case where the most probable thermal speed equals the orbital speed); and 8:1 (a typical case where the orbital speed is eight times the most probable thermal speed). The polar plot emphasizes the "beam" concept, while rectangular plots and their integrals are more easily applied to effects resulting from atomic oxygen exposure.

Since the temperature of the thermosphere is strongly dependent on solar activity, both high and low solar activity cases are shown (Figure 5.6-3). It should be noted that, unlike Nocilla, we have normalized the maxima of all distributions to unity, so only percentages of maximum as a function of angle are displayed. This simplifies presentation, since the lobe for the 8:1 ratio (Figure 5.6-2), normalized according to total fluence (equal areas for equal fluences), would have a much larger maximum than the others. Also, the maximum etch depths would be greatest for solar maximum conditions that produce the largest densities of ambient oxygen atoms.

The cosine distribution (Figure 5.6-2) agrees with the limiting case for effusion of gases through an orifice where both the gas ensemble and the orifice are stationary. The progressive elongation of the angular distribution with speed ratio is also consistent with observations. Such angular distributions can be used to visualize the "spread" that particles exhibit after passing through a small area or to describe the angles of incidence on differential areas on forward-facing surfaces. It is apparent from a rectangular plot of a typical angular distribution (Figure 5.6-3) that few atoms strike forward-facing surfaces with angles of incidence

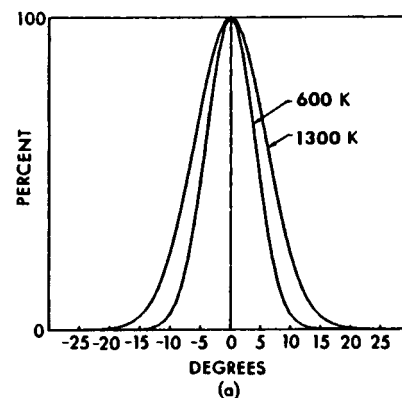
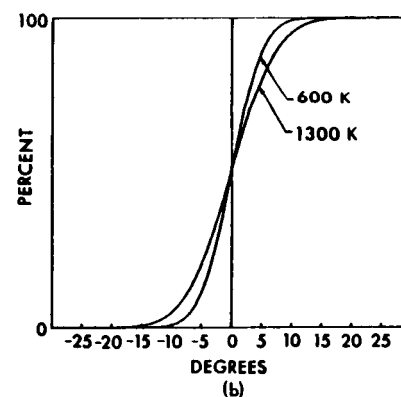


Figure 5.6-3

Rectangular plot of the angular distributions (a) during high solar activity ($T = 1300^\circ\text{K}$) and solar minimum ($T = 600^\circ\text{K}$) conditions. The integral of these distributions (b) relates to the etch profiles.



ORIGINAL PAGE
BLACK AND WHITE PHOTOGRAPH

Figure 5.6-4

Scanning electron micrograph of an etched CR-39 plastic surface showing edge profiles where a knife-edged cover was located and where a Nb thin film is still located (photo by A. Dorries).



exceeding 15° off-normal.

A number of theoretical etch profiles have been examined (Figure 5.6-1). For a surface located behind a slit at a distance large compared to the slit width, the etch profile perpendicular to the slit should have the shape of an inverted angular distribution (Figure 5.6-1a).

The situation for an elevated half-plane mask is somewhat different (Figure 5.6-1b) in that etched area approaching the edge of the half-plane from the right receive progressively less fluence (more area under the distribution curve is blocked). Vertically under the edge all atoms incident from the left of the edge have been blocked, reducing the maximum fluence by one-half. This reduction in fluence continues under the overhang until the effective limit for incidence angles is reached. Since the fluence at any point on the etched surface is a summation of atoms for all angles of incidence permitted at that point, it is observed that unshadowed area receive fluences proportional to the total area under the angular distribution curve (Figure 5.6-3), while a partially shadowed surface receives a fluence at each point on the etchable surface that is proportional to the area under the angular distribution curve that is not blocked by the mask. Thus, the etch profile for the half-plane mask is equivalent to plotting the integral of the angular distribution function.

The etch profile near a solid step mask (Figure 5.6-1c) resembles that for the half-plane mask for the portion in front of the step, but at the step the front face blocks additional fluence resulting in a nearly vertical decrease in the etch depth at the step (approximately 0.1° maximum undercutting relative to a $560\text{ }\mu\text{m}$ mask height occurs for a $9\text{ }\mu\text{m}$ etch depth). The etch profile (Figure 5.6-1d) that occurs near a solid knife-edge mask with edges sloped greater than 15° from a normal incidence direction, or near a thin film mask deposited on

the etchable surface, is nearly a vertical step.

Scanning electron micrographs, which equally magnify both the horizontal and vertical dimensions, show slightly sloped edges even for the etched steps near thin film masks (Figure 5.6-4). The slopes result from shadowing by slightly elevated knife edges or by self-shadowing by the etch steps. With self-shadowing, the height of the step providing the shadowing is continuously increasing with the etch depth.

The slopes of any etched edges should extend less than 15° relative to the top edge of the shadowing structure for normally incident atoms; thus, the extent of the shadow increases with mask height. A particle, or other contaminant, on the surface would initially mask an area its size, but as etching progresses the shadowed area expands, with most of the fluence shadowing occurring within 7° of the orbital velocity direction and limited essentially to less than 15° . This general profile and limit appear consistent with scanning electron micrographs of etched surfaces (Figure 5.6-4).

One diffuse etch step (oriented vertically in Figure 5.6-4) occurred near a slightly elevated knife edge of an aluminum cover, while another sharp etch step (oriented horizontally in the same figure) occurred at the edge of a niobium thin film pattern deposited on the surface prior to etching. Both steps are similar to the profiles in Figure 5.6-1 except the heights of the shadowing structures were small and increased by relatively large amounts with etch depth. Fine microstructures (spiked in region in Figure 5.6-4) are observed on most etched structures (even amorphous plastics) and are undoubtedly influenced by this self-shadowing effect.

It is hypothesized that condensed contaminants, segregated at nucleation sites, or fine particles on the surface provided masking and that

self-shadowing created the sloped sides. Accommodation of the fast oxygen atoms may have a lower efficiency at glancing incidence to the surface so further studies are needed to fully test these hypotheses. Similar structures have been observed on ground-based ion-bombarded surfaces¹. Precleaning has eliminated such structures in semiconductor device fabrications⁹. Thermal and ensemble velocities, from electrical accelerations in ground-based sputtering plasmas, should create shadowing effects similar to those in orbit.

Actual stylus tracings of some samples flown on STS-8 are shown in Figure 5.6-5. One tracing (Figure 5.6-5a), which was taken from a vitreous carbon surface that was at the base of 560 μm -thick solid step, is typical for near alignment of the step with the orbital direction (within 0.5°). Corrections for a chipped edge, an error due to the stylus shank contacting the etch step, and contaminant created peaks are shown by a dashed line (Figure 5.6-5a). Other examples where the mask step faces were not aligned with the orbital direction are shown (Figures 5.6-5c and 5d), and the excellent steps obtained with niobium thin film masks (Figure 5.6-5b) demonstrate the advantages of this type of mask for determining etch rates and reaction efficiencies, especially for rapidly etched materials such as the polycarbonate (CR-39) shown in Figure 5.6-5b.

The measured etch profile was digitized and compared to computed etch profiles for different ambient gas temperatures. These were obtained by normalizing the maximum fluence to the maximum etch depth observed and requiring half etch depths to align laterally at zero angle of incidence (Figure 5.6-6). This procedure indicated that the average temperature of the oxygen atoms was $750 \pm 50^\circ\text{K}$ for the best fit.

Discussion

The range in angular distribution of gas particles incident upon a satellite strongly influences observed degradation effects and surface morphologies produced. Surfaces facing the forward or "ram" direction are subject to heavy erosion in low Earth orbits if they are combustible and unprotected. The erosion may also be used as a quantitative sensor of atomic oxygen³. The usual treatments of equilibrium thermodynamic variables, such as pressure and temperature, have to be modified for observations in orbit. Except for outgassed or accommodated species traveling with the satellite, the orbital velocity dominates relative collision speeds between neutral, thermospheric species, and the orbiting surfaces.

Atoms reflected from the iron faces of mask steps could be a source of additional etching, but small cross sections and broad scattering (due to accommodation) appear to reduce this effect below the accuracy of the profile measurements discussed here; however, higher sensitivity reflection measurements of a different nature will soon be reported.

The theoretical and measured etch profiles matched extremely well considering that the etched surface received a total fluence that was integrated over 41.2 hours with contributions from various latitudes and during day and night conditions. During the STS-8 mission, ambient temperatures varied from approximately 690°K to 1000°K based on extreme conditions and application of mass spectroscopy incoherent scatter (MSIS) and MSFC/J70 thermospheric models. An estimated average of $825 \pm 165^\circ\text{K}$ resulted from the latter model.

Summary

Theoretical angular distribution profiles for oxygen atoms incident to surfaces or exiting behind masks have been calculated in an orbiting

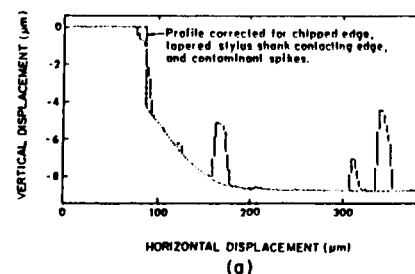
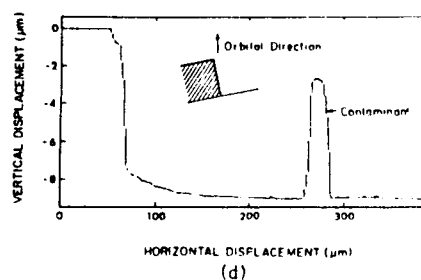
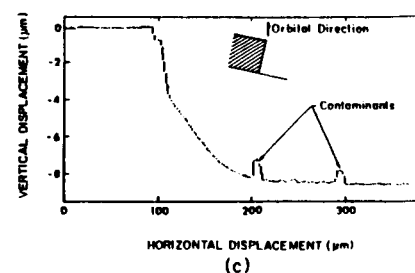
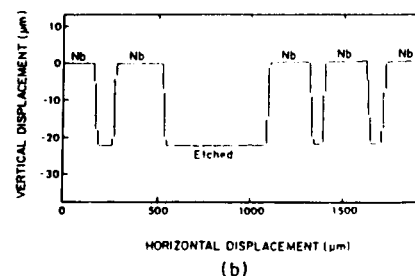


Figure 5.6-5

Stylus profilometry tracings taken from samples flown on STS-8. Profiles (a), (c), and (d) are from etched vitreous carbon near solid step masks, and (b) is from a polycarbonate plastic surface on which a niobium thin film pattern was deposited.



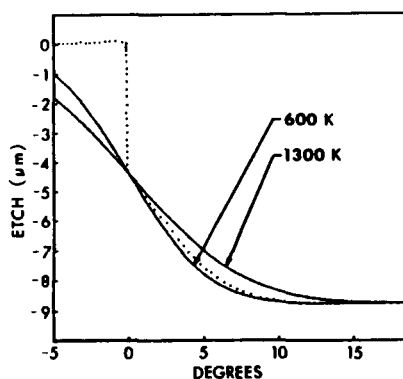


Figure 5.6-6

Comparison of a measured etch profile (partially corrected for: chipped edged, contaminants, and stylus shank contacting step edge) with the theoretical profiles for 600 °K and 1300 °K ambient temperatures. Best fit to measured profile occurs for 750 ± 50 °K.

reference frame. These profiles are dependent upon the ratio of the orbital speed to the most probable thermal speed of the ambient oxygen atoms. The profiles of etched combustible surfaces have been measured and related to such distribution profiles and a temperature of 750 ± 50 °K, consistent with the mean ambient temperature at this altitude and for the solar activity during exposure, was obtained. Calculated profiles for a number of mask/substrate configurations were given. The method can be applied to other experimental conditions including those in terrestrial simulators where the ensemble velocity and effective gas temperature may be independently carried. Structures of variable shape may thus be produced on surfaces.

Acknowledgement

This work was performed in collaboration with P. N. Peters and C. Sisk of the Space Science Laboratory NASA, MSFC.

References

1. Auciello, O., and R. Kelly, (Eds.), Ion Bombardment Modification of Surfaces, 466 pp., Elsevier, New York, 1984.
2. Gregory, J.C., and P.N. Peters, "Interaction of Atomic Oxygen with Solid Surface at Orbital Altitudes" (A0114), in The Long Duration Exposure Facility (LDEF),

NASA SP-473, edited by L.G. Clark, et al., 14-18, 1984.

3. Gregory, J.C., and P.N. Peters, "The Production of Glow Precursors by Oxidative Erosion of Spacecraft Surfaces," in Second Workshop on Spacecraft Glow, NASA CP-2391, edited by J.H. Waite, Jr., and T.W. Moorehead, 174-179, 1985.
4. Leger, L.J., Oxygen Atomic Reaction with Shuttle Materials at Orbital Altitudes, NASA TM-58246, May 1982.
5. Nocilla, S., "The Surface Re-emission Law in Free Molecule Flow," in Rarified Gas Dynamics, edited by J.A. Laurmann, 327-346, Academic Press, New York, 1963.
6. Peters, P.N., R.C. Linton, and E.R. Miller, "Results of Apparent Atomic Oxygen Reactions on Ag, C, and Os Exposed during the Shuttle STS-4 Orbits," *Geophys. Res. Lett.*, 10, 569-571, 1983.
7. Peters, P.N., J.C. Gregory, and J.T. Swann, "Effects on Optical Systems from Interactions with Oxygen Atoms in Low Earth Orbits," *Applied Optics*, 25, 1290-1298, 1986.
8. Visentine, J.T., L.J. Leger, J.F. Kuminecz, and I.K. Spiker, "STS-8 Atomic Oxygen Experiment," AIAA Paper No. 85-0415, 1985.
9. Wang, D., and J. Wong, "Etched Trenches Conserve Semiconductor Device Space," *Res. & Dev.*, 27, 107-112, 1983.

Project: Powdered Metal Sintering and Infiltration

Industrial Participant: Tripty Mookherji, Teledyne Brown Engineering, 300 Sparkman Drive, Huntsville, Ala.

UAH: James E. Smith, Jr., Department of Chemistry

Introduction

This task examines the influence which low gravity has on reactive liquid phase sintering of intermetallic alloys in a solid phase matrix of refractory metal (W or WC). Particular emphasis is being placed on those powdered metal compacts which produce liquid alloys on sintering. For this case of materials, heating to a two phase region causes the constituent components to react, forming an alloy liquid which must wet the solid phase. Densification is initially driven by the free energy effects which cause rapid rearrangement. Further densification occurs by evaporation and condensation, surface diffusion, bulk flow, and volume diffusion.

In unit gravity, sedimentation causes stratification within the sample that results in a non-uniform coarsening of microstructure. Sintering, in a reduced gravity environment, should produce a smaller grain size, a more uniform microstructure (possibly with fewer voids or defects) and improved mechanical properties.

Potential uses for liquid-phase sintered products include bearings, magnetic materials, electrical brushes and contact points, advanced cutting tools to cut at higher linear speeds than currently possible, irregular shaped mechanical parts for high stress environments, and possibly new and improved catalysts for chemical production.

Sounding rocket experiment

During the past year, this project has focused on the conception, design, fabrication, and testing of a

sounding rocket experiment to perform powdered metal sintering in a low gravity environment. A furnace was designed and an experiment conceived to facilitate powdered metal sintering in the 5 to 6 minutes of low-g offered by a sounding rocket. The furnace will process from 4 to 5 samples simultaneously at temperatures approaching 1600°C. This high temperature, about 2.5 times the melting point of the rocket airframe, required considerable engineering to protect the airframe during flight. The exterior of the furnace casing and its base plate are both water cooled at a flow rate of 0.5 cm³/sec. Helium is used to protect the sample during all phases of heating and cooling, as the refractory metal compact oxidizes easily. The melting point of the minority phase, composed of iron and titanium powdered metal mixtures, forms reactive liquid alloys at temperatures exceeding 1500°C. Because of the high operating temperature and large thermal mass, the furnace must be launched preheated at a temperature of 1400°C.

Once low-g is achieved, the furnace temperature will be raised to 1600 °C in 2 minutes or less to melt and alloy the minority phase. The heater is turned off and the sample soaked for 30 seconds. The 30 seconds eliminates any influences which the electrical field might have on the samples being processed and permits time for the samples to approach an equilibrium temperature. Finally, a high flow rate of helium is used to quench the sample and solidify the minority phase prior to re-entering gravity. A portion of this helium, flows through special ports in the insulation, heating coils, and internal covers before being exhausted through a non-propulsive vent. This helium is used to begin cooling of the furnace for recovery and to prevent the re-melting of the sample once the quench is discontinued after 2 minutes. A slow flow of

5.7 Powdered metal sintering

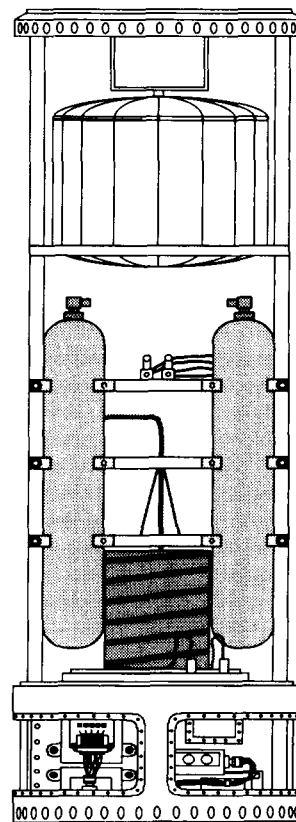


Fig. 5.7-1
Diagram of furnace section of Consort 1 payload.

helium is resumed and continues for up to 4 hours after launch to protect the samples from oxidation while the furnace cools.

Figure 5.7-1 show a drawing of the

Table 5.7-1

Timeline for Powdered Metal Sintering Experiment

TIME*	EVENT
-335 min.	Begin external flow of helium for environmental conditioning of sample (50 cc/sec STP)
-300 min.	Begin external flow of cooling water (0.53 cc/sec)
-290 min.	Begin external heating at 5°C/min from ambient temperature to 1400°C
-290 min.	Begin nitrogen purge of the furnace section (130 ft ³ /min STP)
-15 sec.	Activate relay to switch to internal power**
-15 sec.	Activate latching relay and solenoid valve to switch to internal flow helium (50 cc/sec STP)**
-2 sec.	Activate latching relay and solenoid valve to switch to internal flow of cooling water (0.53 cc/sec)**
T-0	Launch**
+1 min.	Begin heating from 1400 to 1600°C at 0.01 g
+3 min.	Disengage furnace power
+3.5 min.	Activate high-speed helium relay and solenoid valve to begin helium quench at a flow rate of (4930 cc/sec STP)
+6 min.	Disengage high-speed helium flow relay and solenoid valve
+240 min.	Disconnect furnace battery pack

* Referenced to launch

** This schedule assumes no interruptions in power. If interruptions occur, the furnace must be given additional time to achieve its required pre-launch temperature of 1400°C.

Table 5.7-2

External cooling and electrical requirements

1. Helium
 - a. Purity = 99.999% minimum.
 - b. Flowrate = 50 cc/sec.
2. Water
 - a. Demineralized.
 - b. Flowrate = 0.53 cc/sec.
3. Nitrogen or Dry Air
 - a. Dry.
 - b. Cool module before launch.
 - c. Flowrate = 120-150 ft³/min
4. 28 VDC
 - a. 5-15 amps.

major components of the furnace section of the sounding rocket payload. The water tank contains a pressurization bladder and 9 liters of demineralized water which is used to protect the air frame from 15 seconds before launch to up to 4 hours after launch. Four 3-liter tanks of helium provide the slow flow rate of helium needed to protect the sample from oxygen and gas for the 2-minute quench needed to solidify the minority phase. The furnace is shown in the lower portion attached to its water cooled base plate which is, supported by a mounting plate. The figure does not show the valving mechanism or relay support rack which is suspended just below the mounting plate. On this rack are

positioned three solenoid valves to permit switching to internal helium, water, and facilitate the high helium flow rate. Since the tanks of helium will be pressurized to approximately 1800 psia, a regulator is needed to reduce the pressure to the 25-35 psia over-pressure required to protect the samples and furnace. This regulator is also positioned on this rack. Temperature measurement is by way of a W/Re thermocouple referenced to a thermistor. Amplification and conditioning of this signal is accomplished by a circuit located on this rack before the signal is sent to the main controller. In addition to these components, the main relay for switching from external to internal power and the SSR used to control the furnace are also located on this rack.

Table 5.7-1 details the requirements for the mission. Ground power preheats the furnace, providing the large amount of heat needed to achieve a steady state, prelaunch temperature of 1400°C. Fifteen seconds before launch, power is provided by an onboard dedicated battery located above the water tank in Figure 1. Nitrogen or dry air will be used to cool the rocket module which houses the furnace while the rocket is on the ground. Table 5.6-2 outlines the electrical and cooling requirements for the mission.

Furnace development

The initial flight furnace design was a hybrid of the Automated Directional Solidification Furnace (ADSF) and the experimental package from the Isothermal Casting Furnace (ICF) flight furnace. Following the first vibration test, components were found to have suffered abrasion damage with one component virtually decomposed. The extreme vibrational and high-g loads offered by the sounding rocket forced the re-design of all of the zirconia insulating components and support members. The re-designed

ORIGINAL PAGE BLACK AND WHITE PHOTOGRAPH

furnace was subjected to a second vibration test and upon inspection no damage was found. A third vibration test, with the furnace preheated to 1400 °C is planned.

Sample preparation

The sounding rocket experimental furnace was constructed to sinter material with dimensions identical to those used in the existing high temperature sintering furnace and the environmentally controlled sintering press which is under development. The high temperature sintering furnace has been completed and has undergone preliminary tests to verify control performance and map the furnace zones. The environmentally controlled sintering press (ECSP), which was partially complete and described in last year's annual report, has been fully instrumented and interfaced to an IBM-compatible PC. The ECSP will be used to prepare four or five samples of iron (2 cm diameter x 2.54 cm long) and titanium powders dispersed in either a W or WC majority phase. The concentrations and ratios of iron and titanium will be varied in the samples to be processed both in flight and on the ground in the high temperature sintering furnace.

Before preparing these samples, the ECSP control program had to be written and fully tested. Four independent heaters are monitored by type-K thermocouples. An additional thermocouple monitors the die temperature, which is assumed to be the temperature at which the compact is processed. A preliminary test of the control program was conducted on an aluminum sample sintered at 25,000 psia for 18 minutes at a set point temperature of 100 °C. Refractory metal compacts were not used for this test because of their expense. PID control algorithms were incorporated in the BASIC program written for the ECSP. Figure 5.7-3 shows the initial performance and control of the three finger

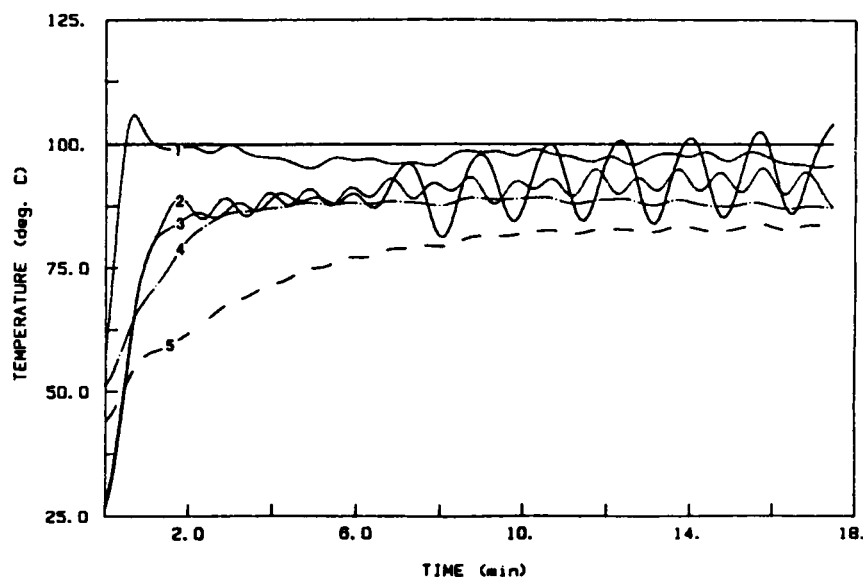
heaters used to heat the plunger (1) and base plate (2,3), the main heater used to heat the die (4), and die or process temperature (5). Three of the heaters (2,3,4) indicate that the proportional component of the PID function operated successfully and that further increases in the integral and derivative constants in the function need to be made. The plunger heater (1) shows an under-damped response which can be corrected by adjusting the value of the proportional constant.

The process temperature, on the other hand, shows the critically damped behavior which was desired. This initial ECSP thermal performance test demonstrated that the control program functions correctly and that the parameters used in the control algorithm are in need of further tuning. Pressing parameters, namely, applied pressure, sintering temperature, and holding times for the refractory compacts need to be determined and are subjects of further studies. In addition, the high temperature sintering furnace zones will be mapped to determine axial temperature profiles.



Figure 5.7-2
Ground-based version of the Consort 1 sintering furnace.

Figure 5.7-3
Temperature vs. time response of ECSP processing an aluminum sample.



5.8 High-temperature superconductors

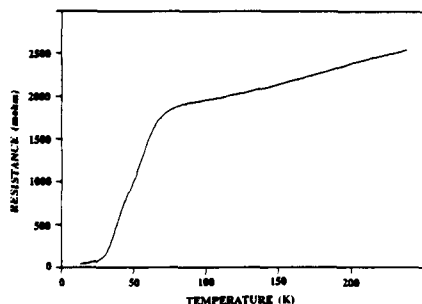


Figure 5.8-1
Electrical resistance of the annealed 123 film as a function of temperature.

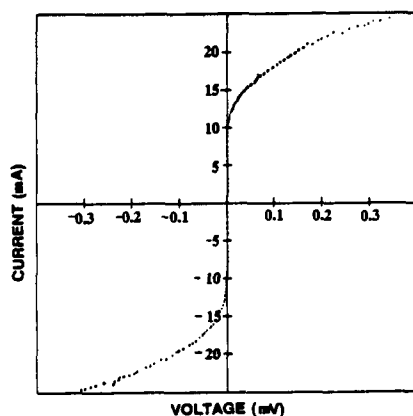


Figure 5.8-2
I-V characteristics of annealed 123 film.

Project: High Temperature Copper Oxide Superconductors
UAH: Maw-Kuen Wu, Boon H. Loo, Department of Chemistry*

Introduction

During the past year, major advances have been made in the fabrication processes and characterization techniques of high T_c superconductors; these are described below. Some experiments were made in collaboration with P. N. Peters and R. C. Sisk of NASA-Marshall Space Flight Center in Huntsville, Alabama, and with C. Y. Huang of the Lockheed Research and Development Division in Palo Alto, Calif.

Superconducting thin films

The RF sputtering technique was used to fabricate thin films. The 123 target material was first annealed in oxygen at 950°C for six hours, then slow-cooled in the furnace. Its superconducting onset temperature was typically about 96°K. The 211 substrate material was prepared by heating and regrinding Y_2O_3 , BaO, and CuO several times to ensure complete reaction. Homogeneity of the 211 phase was determined using a Raman microprobe.

The initially sputtered film was about 1 μ m thick and was initially semiconducting. It became superconducting after oxygen annealing at 900°C for 30 minutes and furnace-cooling. Figure 5.8-1 shows the resistance of the annealed film as a function of temperature. The superconducting transition was at 93°K and sharp. The film's I-V characteristic is shown in Figure 5.8-2. The critical current density is approximately 350A/cm². This relatively low critical current can be attributed to the substrate materials which were prepared with the conventional powder sintering technique. A compact substrate or even a single crystal 211 should give better films. The advan-

tage of using a 211 substrate is that the transition temperature of the annealed sputtered film did not degrade. The relative ease of making the 211 substrate and the simple preparation conditions also make it a more attractive process.

High temperature processing

Green 211 Phase: Sintered 211 phase was used as the starting material for this work. Firing the sintered disc at 1300°C for 15 minutes converted some of the green phase into black phase. Raman microprobe analysis indicate this black phase is that of $YBa_2Cu_3O_7$. The as-sintered sample had low resistivity at room temperature and behaved like a semiconductor, as shown in Figure 5.8-3(a). The sample became superconducting, as evidenced in Figure 5.8-3(b), after it was oxygen-annealed at 950°C for several hours and furnace-cooled. Some other rare earth 123 phases have been produced from their corresponding 211 phases using the same processing methods.

The thermodynamics of the system at temperatures higher than 950°C have not been thoroughly investigated. Our results suggest that the 123 phase is more stable than 211 at higher temperature. In view of these observations, a detailed study of the equilibrium phase diagram at these temperatures would provide better control for synthesizing the superconducting compound.

Bi-Sr-Cu-O: Early in April 1987, we observed a resistance anomaly at 60°K in the Bi-Sr-Cu-O system prepared at 900°C with 30 minutes sintering time. However, a longer processing time at 850°C of the sample showed a complete superconducting transition at 15°K. We used a high temperature processing technique to re-examine the system. A material with nominal composition of $BiSrCuO_{4-y}$ was prepared from Bi_2O_3 , SrO, and CuO, pressed into a pellet, and heated to 800-850°C for 12

*Now with Columbia University.

hours. The sample was quenched, re-ground, and annealed in oxygen for two hours at 1200°C and slow-cooled in the furnace. The samples melted during heating but needle-like crystals were found inside the melt. Figure 5.8-4 shows the temperature dependence of the magnetic moment, \underline{m} , for a sample cooled in fields of 10 and 100 G. Clearly the moment deviates around 60°K, suggesting a superconducting onset at 60°K. This onset temperature is in agreement with the onset of the resistance measurement as shown in the inset of Figure 5.8-4. Figure 5.8-5 shows the field dependence when the sample was cooled in zero magnetic field. At low fields, \underline{m} is linear in \underline{H} , but starts to deviate at higher fields, thus defining \underline{H}_{c1} . The \underline{H}_{c1} value at 7°K is 20 G. As shown in Figure 5.8-4, \underline{m} is positive above T_c , indicating the presence of magnetic moments which are presumably caused by the presence of Cu^{2+} from unidentified phases. These moments might be the reason that \underline{m} crosses zero at relatively low field values, as shown in Figure 5.8-5. X-ray and Raman microprobe analysis (Figure 5.8-6) of these materials differed from both those of the 214 and 123 phases, indicating the possible existence of a new phase. Structure determination of this system is currently underway.

Two important conclusions can be drawn from this study. First, ions other than rare earth metals can form new copper oxide compounds that still exhibit high temperature superconductivity. Second, high temperature processing may be favorable to the formation of certain high temperature copper oxide systems.

Y-Sr-Cu-O: Complete replacement of the Ba^{2+} ions with the smaller alkaline earth metal ions has not produced high- T_c superconductors. Thus far, only $\text{Y}_{0.3}\text{Sr}_{0.7}\text{CuO}_{3-y}$ with a T_c of about 40°K has been reported. Based on the successful results on Bi-Sr-Cu-O system, we decided to re-

examine the Y-Sr-Cu-O system using similar high temperature processing conditions.

A sample with a nominal composition YSrCuO_{4-y} was prepared by mixing appropriate amounts of Y_2O_3 , SrO , and CuO . The mixture was ground and pressed into pellets, heated to 1300°C for 2 hours, and then quenched to room temperature (RT). The material was then re-ground, pressed, and reheated to 1200°C for 6 hours in O_2 , and then slowly cooled to RT. High purity alumina crucibles were used in the sample preparation.

The temperature dependence of magnetic moment for a YSrCuO_{4-y} sample (25 mg) cooled in 10, 20, and 50 G are displaced in Figure 5.8-7.

The superconducting onset is about 80°K, which is consistent with that of the resistive one as shown in the inset. A linear temperature dependence of \underline{R} before the onset of superconductivity was observed. The resistance curve of our sample does not indicate the presence of a second superconducting phase. However, the I-V curve clearly reveals the existence of two superconducting phases, as shown in Figure 5.8-8. In addition, measurements of the dc magnetic moment (\underline{m}) on a 25-mg sample also indicated a superconducting transition at 80°K, and another at 40°K (Figure 5.8-8).

The 80°K superconducting phase did not form when our samples were prepared at a lower temperature. This indicates that the 80°K phase is thermodynamically stable only at higher temperatures. This is in consistent with the conversion of the green 211 phase to the corresponding 123 phase with good superconducting characteristics by processing at 1300°C.

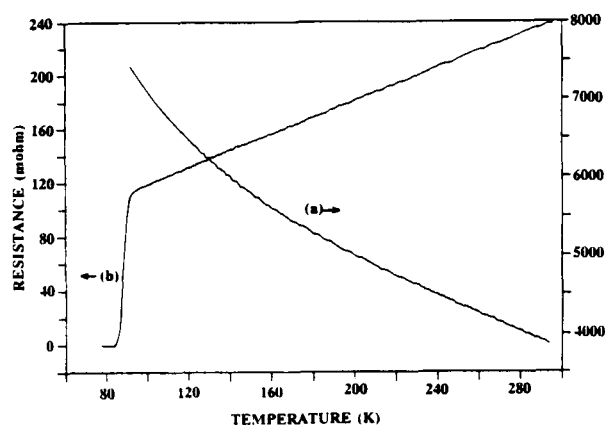


Figure 5.8-3

Resistance curve of a sintered Y_2BaCuO_5 disc after firing at 1300°C and (a) without O_2 anneal and (b) with O_2 anneal.

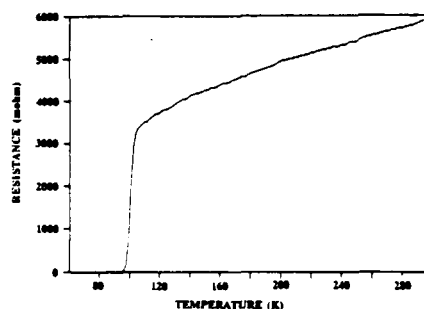


Figure 5.8-4

Resistance curve of sample with nominal composition BiSrCuO_{4-y} .

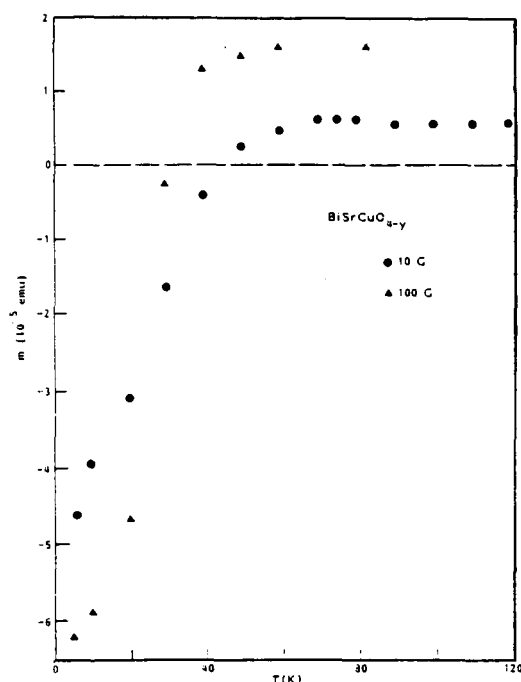


Figure 5.8-5
Magnetic moments of BiSrCuO_{4-y} at 10 G and 100 G.

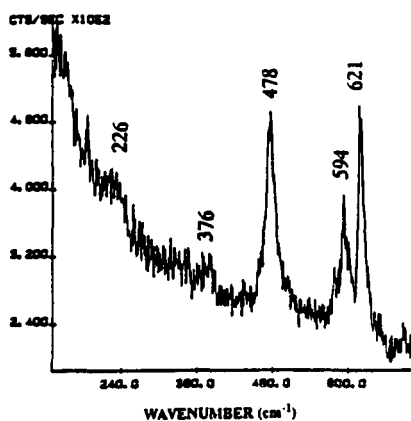


Figure 5.8-6
Raman spectra of BiSrCuO_{4-y} .

In addition to the two superconducting transitions, the magnetic moment curve shows an anomaly at low temperatures. Figure 5.8-9 shows the details of the low temperature data for the sample cooled in 220, 50, 100, 200, and 1000 G. The magnetic moment is diamagnetic for $T < T_c$, but there is a sharp reduction in the diamagnetic moment at 14°K, indicating a sharp drop in superconductivity. It is not likely that this is caused by the onset of magnetic ordering, because the moment above T_c is small. At present, it is not clear whether there is a structural phase transition at this temperature or the presence of an unidentified phase.

$\text{YBa}_2\text{Cu}_3\text{O}_7$ - AgO composite: AgO decomposes when it is heated above 200°C and does not react with high T_c superconductors. Therefore, a $\text{YBa}_2\text{Cu}_3\text{O}_7$ composite can be formed by mixing $\text{YBa}_2\text{Cu}_3\text{O}_7$ and AgO powders, then processing them under appropriate conditions. Because of the high conductivity of the silver component the $\text{YBa}_2\text{Cu}_3\text{O}_7$ -AgO composite may exhibit better superconducting characteristics than the plain $\text{YBa}_2\text{Cu}_3\text{O}_7$ material.

We have successfully synthesized the $\text{YBa}_2\text{Cu}_3\text{O}_7$ -AgO composites in several weight ratios. Some of the typical resistance curves are shown in Figure 5.9-10. It should be noted that the room temperature conductivity increases as the silver content increases. Measurements of critical current density showed that J_c of 250 to 350 A/cm² at 77°K were about two orders of magnitude higher than for our undoped samples at the same temperature. We have also observed a stable suspension of the samples in the divergent field of magnets. While superconducting, they can be suspended above (the normally ob-

served case) or below the magnet. When suspended below, attractive forces equal to the weight plus any repulsion is provided by flux pinning. A total weight of 2.07 times the sample weight was successfully lifted from a 77°K surface with a magnet having a maximum field of 3.3 kG and maximum gradient of 2.6 kG/cm.

The M-H hysteresis loop for sample (weight ratio 3:1) measured at 77°K is shown in Figure 5.8-4 to a maximum field $H_{\text{max}} = 0.9$ kOe. It was taken after the sample was cooled in zero field, and was independent of the sweep rate between 0.03 and 0.4 kOe/min. The critical current density estimated from the magnetization at 0.1 kOe is 3.3×10^3 A/cm², based on Bean's critical state model. This value of J_c is an order of magnitude larger than that measured from transport properties. The residual magnetization is 3 emu/g, and is not sensitive to the maximum field larger than 0.5 kOe.

A number of conclusions can be drawn from our observations. The decrease in normal state resistivity and the increase in critical current density with the addition of silver oxide suggest a lowering of contact resistances between grains. Near-identical T_c 's suggest that grain interiors experienced little change. We model the magnetic properties and suspension results in terms of many weak-link current loops, where the weak links are associated with the inter-grain contacts. When a sample is brought into the gradient field of a magnet, the increasing field induces diamagnetic currents in all loops. When a critical current is exceeded in some loop, flux enters that loop, dropping the current momentarily and trapping the flux. Bringing the sample closer to the magnet results in additional flux trapping in weaker loops and further diamagnetic current growth in stronger loops. The induced diamagnetic currents generate repulsive forces in the gradient

field. If at any point in this process the sample moves away from the magnet, the changes in currents and field reverse. Loops with no trapped flux continue to cause repulsion, which is decreasing. However, the currents in the loops with trapped flux will decrease and eventually reverse direction, attempting to prevent flux flow out of the loops; this generates an attractive force in the gradient field. Doping with silver oxide enhances the critical currents of inter-grain contacts, providing stronger pinning forces that can provide the suspension of the sample beneath the magnet. Recent magnetization measurements confirmed that the current density of the composite materials was enhanced by almost two orders of magnitude as compared with the undoped samples.

Summary

The studies presented here indicate that proper processing procedures are critical to the formation of high temperature copper oxide superconductors. Superconducting 123 films can be fabricated using the green 211 phase as a substrate. The superconducting characteristics of these films, in terms of superconducting transition width, are better than the characteristics found when other oxide compounds are used as substrates. A compact or single-crystal 211 phase will be desirable as a substrate for high quality thin films. A new high T_c copper oxide compound with non-rare earth elements was prepared using high temperature processing. High temperature processing presents an alternative synthetic route in the search for new high T_c superconductors.

A $\text{YBa}_2\text{Cu}_3\text{O}_7\text{-AgO}$ composite with improved electrical conductivity and strong flux pinning was also prepared.

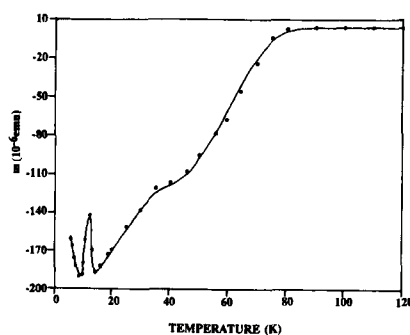


Figure 5.8-7

Temperature dependence of magnetic moment of $\text{YSrCuO}_{4-y'}$

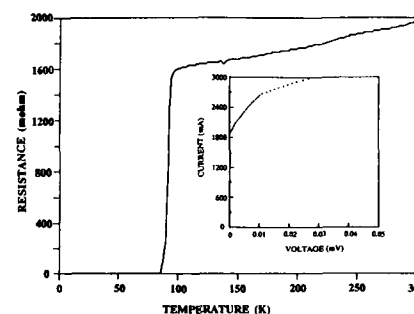


Figure 5.8-8

Resistance curve of $\text{YSrCuO}_{4-y'}$. (Inset: I-V characteristics of $\text{YSrCuO}_{4-y'}$)

Publications

1. Loo, B. H., M. K. Wu, D. H. Burns, A. Ibrahim, C. Jenkins, T. Rolin, Y. G. Lee, D. O. Frazier and F. Adar, "Raman Spectroscopic Characterization of Different Phases in the Y-Ba-Cu-O System" in High Temperature Superconducting Materials—Preparation, Properties, and Processing, ed. W. E. Hatfield, Marcel Dekker, New York 349 (1988).
2. Wu, M. K., J. R. Ashburn, C. Higgins, A. Hampton, B. H. Loo, D. H. Burns, T. Rolin, D. G. Agresti, "Ion Doping Effects on the 90K Superconducting Perovskite," *Chinese J. Physics*, 26 Suppl. 1, S32, (1988).
3. Wu, M. K., J. R. Ashburn, C. A. Higgins, W. E. Carswell, B. H. Loo, D. H. Burns, A. Ibrahim, T. Rolin, P. N. Peters, and R. C. Sisk, "Study of the High Temperature Oxide Superconductors" in Proceedings of SPIE's Symposium on High Temperature Superconductivity, Vol. 879, Los Angeles, 130, (1988).
4. Wu, M. K., J. R. Ashburn, C. A. Higgins, C. Fellows, B. H. Loo, D. H. Burns, A. Ibrahim, T. Rolin, P. N. Peters, R. C. Sisk and C. Y. Huang "High Temperature Processing of Cuprate Oxide Superconductors," *Appl. Phys. Lett.* 52, 1915, (1988).

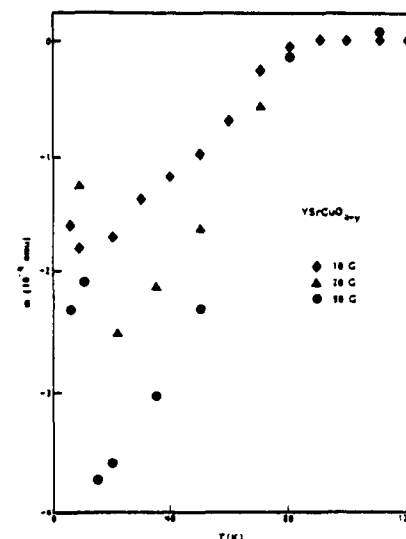


Figure 5.8-9

Magnetic moment of $\text{YSrCuO}_{4-y'}$ at different fields.

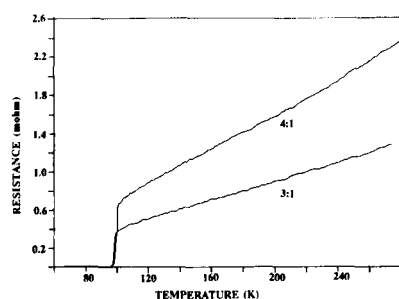


Figure 5.8-10
Electrical resistance of $\text{YBa}_2\text{Cu}_3\text{O}_7$ -
Ag composites. Ratios are in weights
of $\text{YBa}_2\text{Cu}_3\text{O}_7$ to AgO.

5. Wu, M. K., J. R. Ashburn, C. A. Higgins, C. Fellows, B. H. Loo, D. H. Burns, A. Ibrahim, T. Rolin, F. Z. Chien, and C. Y. Huang, "Superconductivity in the Y-Sr-Cu-O System," *Phys. Rev. B.* 37, 9765, (1988).
6. Peters, P. N., R. C. Sisk, E. N. Urban, M. K. Wu and C. Y. Huang, *Appl. Phys. Lett.* (to be published).
7. Wu, M. K., B. H. Loo, *Physica C* 153-155, 908, (1988).
8. Huang, C. Y., K. Shapiro, E. J. McNiff Jr., P. N. Peters, B. B. Schwartz, and M. K. Wu, *Modern Phys. Lett.*, (1988, to be published).
9. Liu, S. H., W. F. Huang and M. K. Wu (submitted to *Phys. Rev. Lett.* 1988).
10. Wu, M. K., J. R. Ashburn, C. A. Higgins, B. H. Loo, D. H. Burns, A. Ibrahim, T. Rolin, P. N. Peters, and R. C. Sisk, *Proceedings of High Temperature Superconductivity Conference*, University of Alabama, Tuscaloosa, AL. (1988).
11. Wu, M. K., B. H. Loo, P. N. Peters and C. Y. Huang, *Proceedings of American Chemical Society*, (1988) (To be published).

Presentations

1. High Temperature Superconducting Symposium in Taiwan, September 1987.
2. US - Japan Symposium on High T_c Superconductivity, Japan, October 1987.
3. American Chemical Society Meeting, New Orleans, September 1987.
4. High Temperature Superconductivity —Fundamentals and Applications, Buffalo, November 1987.
5. International Conference on High T_c Superconductivity, Interlaken, Switzerland, February 1988.
6. Gordon Research Conference, New Hampshire, July 1988.
7. International Symposium on High Temperature Superconducting Materials, Chapel Hill, N.C., September 1987.
8. Pittsburgh Conference and Exposition, New Orleans, Louisiana, February, 1988.

5.9 Wake shield

Project: Wake Shield
Industrial Participant: Wyle Laboratories, P.O. Box 1008, Huntsville, AL 35807-5101
UAH: Gerald R. Karr, Charles Chiu, Department of Mechanical Engineering

Introduction

In cooperation with Graeme Bird of Killara, New South Wales, Australia, a computer program was generated to calculate the flux in the backward-facing region of a wake shield. Charles Chiu has modified this program to better suit the wake shield calculations. The programs run in

Lahey F77L Fortran on a PC with 4 megabytes of memory.

The first program will set up cell geometry, initial conditions (uniform for this case), boundary conditions (specular or diffuse reflection, and generate positions and velocities of simulated molecules. The second will calculate the movements and collisions of simulated molecules until they reach equilibrium, and sample the macroscopic properties by time average. The third will print general properties of molecular species, interpolates pressure on wake shield.

No further work on this project is contemplated in fiscal 1989.

Project: Polymer Foam Processing
Industrial Consultant: Deborah J.

Weiker, Hercules Inc., Research Center, Wilmington, DE 19894.

UAH: Samuel P. McManus, John W. Matthews, Department of Chemistry; Francis C. Wessling, Department of Mechanical Engineering

Introduction

Because of their insulating and mechanical properties, polyurethane foams may be prepared in space in connection with the construction and deployment of the Space Station. As a result, there is interest in determining the effects of space processing on foam properties. With Hercules, Inc. as an interested consulting participant, we have proceeded to define microgravity experiments which would allow evaluation of gravity effects on two-component polyurethane foam production. Hercules has assisted in defining a test system and has agreed to follow the experiments and assist in analyzing the results.

During the past few months we have designed and fabricated hardware for an experiment planned for the Consort 1 rocket flight in 1989. This experiment, which is designed to evaluate the effect of microgravity processing on foam properties, involves preparation of a rigid two-component polyurethane foam. One component is a commercial diisocyanate formulation of monomeric and polymeric diisocyanates based on the diphenylmethane-4,4'-diisocyanate structure. The other component includes a sucrose-based polyol, a silicone surfactant, a basic catalyst, and a Freon blowing agent. Numerous laboratory mixes have been evaluated at UAH and at Hercules, Inc. in order to choose the composition to be evaluated. A laboratory model of the flight hardware was constructed and many test runs have been carried out with various configurations of injection orifices, mixing chamber, and exit chamber.

Additional experiments are planned to evaluate the effect of gravity on foam properties. Some high-g ($>1g$) experiments have been carried out to allow extrapolation of low-g effects. Results of those experiments will be fully analyzed during the fall of 1988. Preliminary analysis reveals that gravity does effect the process. Phase separation is obvious at higher gravity levels. With these samples and with the materials prepared at low gravity levels, a series of tests will be carried out. The foam will be sectioned and evaluated under the microscope to determine the size, shape, and regularity of cells. Also, the percentage of closed to open cells will be determined. Finally, the density, thermal conductivity, and mechanical strength will be determined.

We are also investigating other types of foams as materials to be evaluated at variable gravity levels. In particular, we are considering preparation of a foam from a thermoplastic substance like polyethylene. Such foams are well known and are made from the plastic by heating the substance above its softening point to release blowing and cross-linking agents which are intimately mixed (dissolved) in the plastic. In a microgravity environment, one should be able to prepare an extremely uniform foam with small, regular cells. An experiment utilizing this approach will be planned during the coming year.

5.10
Polymer foam



Figure 5.10-1
Foam experiment apparatus for flight on Consort 1.

ORIGINAL PAGE
 BLACK AND WHITE PHOTOGRAPH

5.10.1 Elastomer-modified epoxy resins

Project : Elastomer-Modified Epoxy Resins

Industrial Guest Investigator: Jon Geibel, Phillips Petroleum Co., Bartlesville, Okla.

UAH: J. Milton Harris, Department of Chemistry, Francis C. Wessling, Department of Mechanical Engineering

Introduction

Our early experiments with demixing of immiscible liquids indicates that the demixing process proceeds unusually slowly in low-g to give spherical domains undistorted by sedimentation. Thus it is of interest to investigate the influence of these demixing differences on the properties of immiscible polymer blends prepared in low g. It is reasonable to expect that domain size and morphology will affect the mechanical properties of the blends.

As a test of this concept we have begun ground-based experiments to support a planned sounding-rocket flight with elastomer-modified epoxy resins. At the initiation of the experiment the resins exist as a single phase. Then heat is applied and catalytic cross-linking begins. As cross-linking proceeds, the elastomer phase separates from the epoxy phase and shortly thereafter the morphology is frozen by solidification. The goal of this experiment will be to examine several of the epoxies with different compositions giving different phase-segregation points. These samples will be examined,

upon their return, for differences in morphology (i.e., domain shape and size) and mechanical strength.

The epoxy used here consists of the bis-glycidyl ether of bis-phenol-A which has been capped with a carboxylated elastomer made of a copolymer of butadiene and acrylonitrile. We are now examining various catalysts for the crosslinking process with the goal of finding a catalyst that does not act for 48 hours at room temperature but that will give complete cross-linking within five minutes; these restrictions come from the necessity to load the rocket some hours or days before launch, then to process the sample in the five to eight minutes of low-g provided by the rocket.

We have designed and constructed an apparatus for performing this experiment in low-g. A major design restriction comes from the need to heat the experiment to 200°C within two minutes and then to hold this temperature for another five minutes. The apparatus consists of a thin mold of epoxy with a series of rectangular cavities containing the resin. This mold is sandwiched by thin aluminum plates which are in turn sandwiched by two silicone-rubber heaters.

The heating regime is controlled by the small computer included in the sounding-rocket experiment. Mold release compound is used to prevent the elastomer-modified epoxy from adhering to the epoxy mold.

5.11 Iron-Carbon Solidification

Project: Iron-Carbon Solidification

Industrial Participant: Norman P. Lillybeck, Deere & Co., 3300 River Dr. Moline, IL 61265

UAH: James E. Smith, Jr., Department of Chemistry

Introduction

The objective of this task is to use the microgravity environment to learn more about fundamental processes that occur in forming cast iron.

This knowledge can then be used to improve cast iron technology on Earth and, thereby, enhance the economic posture of the industrial participant. This task has been held in abeyance at the request of Deere and Co. because of the lack of flight opportunities in the past three years. The sintering furnace to be flown on Consort 1 may provide an opportunity for investigating iron-carbon solidification on a later Consort flight.

ORIGINAL PAGE BLACK AND WHITE PHOTOGRAPH

Task: Measurement of Microgravity Environment

UAH: Jan A. Bijvoet, Robert S. Newberry, CMDS

Introduction

The purpose of this task is to develop means and methodologies to determine very low gravity disturbance levels at experiment locations with an accuracy to meet the needs of various experimenters.

This activity will capitalize on and benefit from the on-going UAH study on "Acceleration Measurement and Management" (for Space Station, etc.) performed for NASA's Office of Aeronautics and Space Technology.

Current activities concentrate on determining the microgravity environment during the coasting part of the flight of the planned Consort 1 flight.

Two 3-dimensional accelerometer systems of different design will be installed at different locations. This will provide the best estimation of the microgravity environment at different experiment locations as well as obtaining redundancy and gaining experience.

Each of the accelerometers will generate output signals for each of three orthogonal axes proportional to the momentary acceleration level. These signals will be sent to the ground in real time by telemetry and to the on-board experiment controller for initiation of experiments. The data will be recorded on-board and on the ground for later analysis.

Development Status

MEA Accelerometer Package: The NASA Marshall Space Flight Center has lent us the spare 3-axis accelerometer from the Materials Experiment Assembly (MEA). This system uses 3 Kearfott 2412 accelerometers and is proven in flight. The theoretical acceleration resolution output is quoted as 10^{-7} g per bit change per

second, but a sample output recording from a previous rocket flight shows a ripple of about 2×10^{-5} g and large spikes. The pulse rate of the accelerometers themselves is 2400 Hz. However, to adapt to the original telemetry system limitations the acceleration data are integrated by the internal data conditioning circuitry to fit a 1 Hz data rate.

This integration significantly reduces the output information content. However no modifications of this proven and reliable system will be made. The MEA accelerometer package has been vibration tested and a few minor problems uncovered and corrected. The MEA accelerometer is ready for integration with the rest of the payload.

UAH Accelerometer Package: UAH purchased three QA-700 accelerometers and a triaxial mounting block from Sundstrand Data Control. The performance of these accelerometers is quoted as $1 \mu\text{g}$ max resolution/threshold and a frequency response from 0-300 Hz. For this CMDS sounding rocket a 1000 Hz wideband FM telemetry link will be used. Therefore all the UAH accelerometer data will be sent to the ground and recorded. The three accelerometers have been mounted on the triaxial mounting block. The integrated system with connections has been vibration tested and no anomalies have been found. The UAH accelerometer package is also ready for integration with the rest of the Consort 1 payload.

Subsequent Activities: Further near term work includes on the ground testing and calibration and the development of the software for processing the acceleration data received from the six channels to determine the low acceleration level and acceleration vector at experiment locations as a function of time, to detect special acceleration events, and to determine the acceleration frequency spectrum.

5.12

Measurement of the microgravity environment



Figure 5.12-1
NASA-MSFC three-axis low-g accelerometer system for Consort 1.

The Consortium for Materials Development in Space is a joint effort of the organizations committed to promoting the commercial exploitation of the space environment. The unique attributes of the space environment offer opportunities for materials processing unavailable to Earth-bound endeavors.

Some activities focus on development of specific materials or pilot processes; other address generic processes or equipment for product development; still others pursue space investigations that generate knowledge having economic value to Earth-based materials processes.

The Consortium is partially funded by the National Aeronautics and Space Administration (NASA) Grant #NAGW-812.

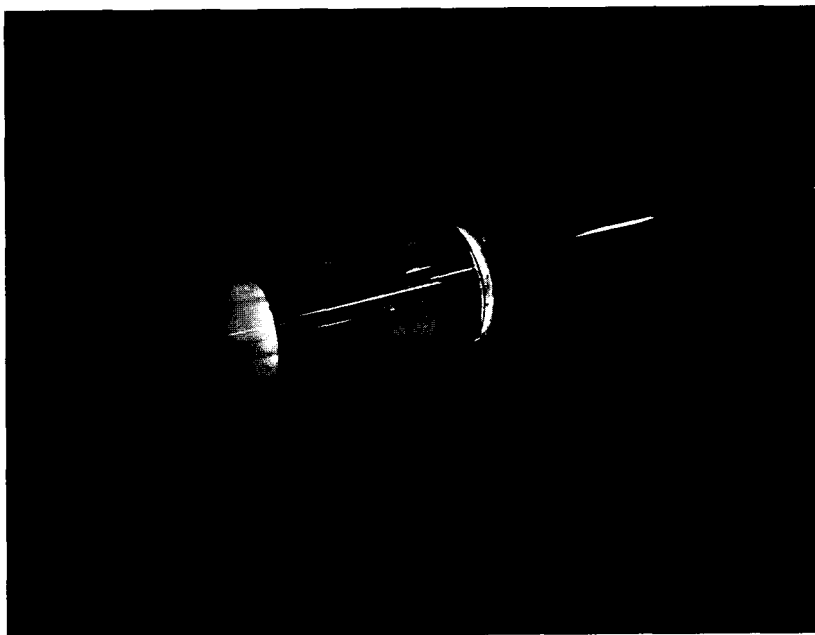
For further information, contact:

Director,
Consortium for Materials Development in Space,
R.I., Box 209
The University of Alabama in Huntsville
Huntsville, AL 35899
205-895-6620

ACKNOWLEDGEMENTS

The staff and members of the CMDS wish to thank Felicia Troupe, Linda Jones, and Gail Patterson of UAH for preparing original manuscripts, Dave Dooling of D² Associates for editing and design, UAH Reproduction Services for printing and binding, and all who supplied reports and illustrations.

On the back cover: *A ground prototype of a furnace for CMDS vapor transport experiments is illuminated by the glow of its own heat (see page 18).*



**The University
Of Alabama
In Huntsville**

An Affirmative Action/Equal Opportunity Institution 978-02674